NASA Contractor Report 3022

Analytical Studies of Separated Vortex Flow on Highly Swept Wings

John M. Kuhlman

GRANT NSG-1357
NOVEMBER 1978

NASA

NASA Contractor Report 3022

Analytical Studies of Separated Vortex Flow on Highly Swept Wings

John M. Kuhlman
Old Dominion University Research Foundation
Norfolk, Virginia

Prepared for
Langley Research Center
under Grant NSG-1357

National Aeronautics
and Space Administration

**Scientific and Technical
Information Office**

1978

SUMMARY

An investigation has been conducted into the capabilities of a subsonic potential flow mathematical model of the flow past slender aerodynamic surfaces with sharp edges and separated vortex flow. Comparisons with experimental data are presented for overall forces and pressure distributions for a series of thin, low aspect ratio wings, including both flat and conically cambered ones. A discussion is presented of the limitations of the current theory, and some suggestions are made as to how the theory might be improved. Details of program data input modifications for three-dimensional geometry are described in an appendix.

INTRODUCTION

The NASA Langley Research Center has had developed under contract by the Boeing Commercial Airplane Company an advanced-panel method for the modeling of a separated vortex flow past a slender, sharp-edged thin wing at subsonic speeds. This method uses distributed doublet singularities located on the actual mean camber surface and the free vortex sheet. The method is referred to as the free vortex sheet theory because the leading-edge vortex is modeled as a sheet of vorticity whose location is free to change in an iteration process to ensure proper satisfaction of the boundary conditions. Early versions of the resulting computer code developed to implement this theory, as described in references 1 and 2, were restricted to incompressible flow.

Also, program storage limitations limited the number of doublet panels on one half of the wing to a maximum of 30. The capabilities of this early code are summarized in references 3 and 4. An extended form of this early code is in the process of being developed. Therefore, this report documents only the code capabilities currently available without attempting to formally document the code in general. Thus, the details of the code or theory will not be described, except to point out that the theory is similar to that discussed in reference 1, with the addition of increased paneling capability and a Gothert rule transformation for the compressible subsonic cases.

Overall force and detailed pressure distribution comparisons between the free vortex sheet theory and experimental data are made in this report for a series of thin low aspect ratio wings of varying planforms. The presented results generally encompass the presently known capabilities of the free vortex sheet code.

NOMENCLATURE

A	aspect ratio, defined as b^2/S
b	wing span, m (ft)
b(x)	local wing span, m (ft)
C_p	pressure coefficient
C_D	drag coefficient
C_L	lift coefficient
C_m	Pitching moment coefficient
c_r	wing root chord, m (ft)
M	Mach number
p	parameter appearing in goemetrical description of wings of reference 15
Re	Reynolds number

S	wing area, m^2 (ft^2)
x	body axis chordwise coordinate, positive downstream, m (ft)
y	body axis spanwise coordinate, positive to the right when viewed from above, m (ft)
z	body axis vertical coordinate, positive up, m (ft)
α	angle of attack
β	sideslip angle

CHARACTERISTICS OF THE PROGRAM

The current free sheet theory has been applied to a variety of low aspect ratio wings; however, only those solutions for which convergence occurs are reported. Convergence has been defined in this report as the sum of the squares of the residuals on the order of 10^{-3}. These residuals are proportional to the nonzero values of the pressure coefficient jump across the shed vortex system(s) and the nonzero values of the normal velocities on the wing panels. The convergence criterion adopted here insures that the worst possible error in the satisfaction of the force-free condition on any one panel on the shed vortex system, assuming all other boundary conditions to be satisfied exactly, is a pressure coefficient difference of 0.03. Similarly, the worst possible nondimensional normal velocity on any wing panel, assuming the force-free shed vortex boundary condition to be satisfied exactly and all other normal velocities to be identically zero, is also no larger than 0.03. It has also been found that convergence is slower at low values of angle of attack for most configurations.

PRESENTATION AND DISCUSSION OF RESULTS

A listing of the various wing configurations studied herein is presented in table 1. Successfully converged solutions are summarized below followed by a discussion of each.

	Figure
1. Aspect ratio 0.52 flat delta wing	1 - 13
2. Aspect ratio 1.0, 70° flat diamond wing	14
3. Aspect ratio 2.0, 70° flat arrow wing	15
4. Aspect ratio 1.6, 80°/65° flat double delta wing	16
5. Aspect ratio 1.147 conically cambered delta wing	17 - 31
6. Flat delta wings at varying aspect ratios	32 - 33

A = 0.52 Delta

The theory is compared with data of references 5 and 6 for a flat, thin, sharp-edged delta wing of aspect ratio 0.52 over a range of Mach numbers of $0.5 \leq M \leq 0.8$. In figure 1 the $C_L - \alpha$ data at M = 0.8 are compared with the free sheet theoretical results over a range of angles of attack of 0° to 30°. Also shown are the theoretical predictions using a vortex-lattice method (references 7 and 8) coupled with the leading-edge suction analogy (references 9 and 10) and denoted by VLM-SA. It is seen that the VLM-SA, also just called the suction analogy, follows the data until $\alpha \cong 20°$, and overpredicts C_L above $\alpha = 20°$. The free sheet theory (square and diamond symbols) shows very good agreement with the data for runs using 42 doublet panels on each half of the wing, while using 30 wing panels leads to a significant underprediction of C_L. Similar results are observed at Mach numbers of 0.5 and 0.7. It was not found possible to obtain converged results for the theory at Mach numbers above 0.8 for this wing.

In figure 2 the lift coefficient results for the separated flow theory are compared with the data of references 5 and 6 and suction analogy for the A = 0.52 flat delta wing at α = 20.8° for a range of subsonic Mach numbers. Both the suction analogy and the separated flow theory predict the observed trend of increasing C_L with increasing Mach number. However, at this α the suction analogy results are four percent high while the separated flow theory results are two percent low relative to the experimental data. The next five figures display the pressure loading details to obtain an understanding of these noted overall differences.

Figures 3, 4, and 5 show the spanwise pressure distributions at Mach numbers of 0.5, 0.7, and 0.8, respectively. The data are at x/c_r = 0.561, while the separated flow theoretical results are slightly ahead at x/c_r = 0.50. However, even with this slight difference in location the theoretical upper and lower surface pressure coefficients agree well with the data from references 5 and 6. Here also it is noted that the agreement with the data is better for configurations having 42 wing panels than for 30 panels.

Figures 6 and 7 are for M = 0.7, at $x/c_r \cong 0.7$ and x/c_r = 0.87, respectively. Again, the theoretical results more closely match the upper surface data when the wing is more finely paneled.

Figures 8 to 10 and 11 to 13 are for M = 0.7, but at other α's, with $x/c_r \cong 0.5$, 0.7, and 0.87 respectively in each group. The theoretical results were only calculated with 30 panels for these α's. Agreement between theory and experiment at α = 10.3° is very good, but at $\alpha \cong 30°$ the theory again underpredicts upper surface pressures.

Theoretical upper surface pressure coefficients near the wing trailing edge are seen in figures 7 and 13 at α = 20.8° and 30°, respectively, to be underpredicted, especially for 30 wing panel configurations. This behavior has been noted in other wing configurations. Such problems are minimized for a fixed number of wing panels by skewing the panel sizes so that there are smaller panels near the wing trailing edge.

70° Diamond

Separated flow theoretical predictions of C_L - α for a 70° leading edge sweep, aspect ratio 1.0, flat diamond wing are compared with force data at $M \cong 0$ from reference 11 in figure 14. The theoretical C_L at $\alpha = 20°$ is in good agreement with the data, while theory underpredicts C_L at $\alpha = 10°$ and $\alpha = 30°$. Also shown are the theoretical results for the augmented vortex lift theory which is developed in reference 12.

70° Arrow

Figure 15 shows C_L - α results for a 70°, aspect ratio 2.0, flat arrow wing. The separated flow theory overpredicts C_L for α between 10° and 30°. The result shown at $\alpha = 10°$ is not well converged; here the sum of the squares of the residuals is of the order 10^{-1}.

Double Delta - 80°/65°

Figure 16 compares the free sheet C_L - α results with data for an aspect ratio 1.6, 80°/65° leading edge sweep flat double-delta wing. Theoretical results assuming separated flow on the strake and attached flow on the wing agree very well with the data for $\alpha \lesssim 12°$, and underpredict C_L for $\alpha \geq 15°$. The free sheet theory, assuming a single shed vortex system emanating from the entire leading edge, agrees very well with experiment for $20° \leq \alpha \leq 30°$, but overpredicts C_L at $\alpha = 10°$ and underpredicts C_L slightly at $\alpha = 5°$. Convergence of these results is to a level of squared residuals that is $0(10^{-2})$, except at $\alpha = 5°$ and 10°, where convergence is $0(10^{-1})$. Shown for comparison is the C_L prediction for the augmented vortex lift theory (ref. 13). Flow past this double-delta configuration was also modeled using two vortex systems: one shed from the strake leading edge, and a second shed from the outboard wing panel. However, convergence was not obtained, and the predicted C_L was approximately 40 percent high. It appeared that the two vortex systems were "hunting" for equilibrium locations.

A = 1.147 Conically Cambered Delta

Figures 17, 18, and 19 compare theoretical predictions of C_L, C_D, and C_m with data from reference 14 for an aspect ratio 1.147, conically cambered delta wing at $M \cong 0$. As described in reference 14, the wing is flat for the inboard 80.5 percent of the local semispan. Outboard of this location the wing is spanwise cambered using a portion of a circular arc, such that the maximum z-elevation or leading-edge droop is 0.105 times the local semispan at all chord stations. Theoretical results shown are for configurations with 63 panels on one-half of the wing. Similar results were obtained at $\alpha = 20°$ for a configuration with 81 wing panels.

Lift coefficient is underpredicted 7.6 percent by the theory at $\alpha = 30°$. The drag polar is very accurate in figure 18; but as seen in figure 17, the angle of attack at which a (C_L, C_D) pair is obtained is slightly overpredicted. In figure 19, the theoretical pitching moment is seen to be too large.

Figures 20 to 31 compare theoretical spanwise pressure distributions with data for the same conically cambered wing from references 14 and 15 at various angles of attack and chordwise stations. Reference 4 has compared similar data for the uncambered A = 1.147 delta with theoretical predictions using the earlier computer code mentioned in the introduction.

Figures 20, 24, and 28 show that the theoretical peak upper surface suction pressures at $\alpha = 10.3°$ are too large, and that these suction peaks are too concentrated in the spanwise direction.

Predictions at $\alpha = 20.4°$, in figures 21, 25, and 29 and at $\alpha = 25.6°$ in figures 22, 26, and 30, and at $\alpha = 30.7°$ in figures 23, 27, and 31 generally agree well with the data on the wing lower surface and on the wing upper surface for nondeminsional wing spanwise coordinates less than 0.8. The theoretical location of the upper surface suction peak at $\alpha = 30.7°$ is noticeably outboard of the peak experimental pressures. For $2y/b > 0.8$, the experimental data show evidence of a secondary vortex which is not modeled by the theory.

Lift-to-drag parameters calculated using the free vortex theory have also been compared, in reference 16, with estimates made using the suction analogy (ref. 8) for the series of conically cambered delta wings described in reference 17. These wings are cambered such that spanwise cuts form a portion of a circular arc.

DESCRIPTION OF KNOWN PROGRAM LIMITATIONS

As shown in table 1, there have been relatively few successfully converged results beyond those discussed in the previous section, and such results fall within the range of α, M, and aspect ratio found previously.

Thus, key limitations in the utilization of the theoretical model are imposed by the poor convergence characteristics of the code for angles of attack less than 10° or greater than 30°, for Mach numbers above approximately 0.80, and aspect ratios above approximately 2.0. These limitations on angle of attack and aspect ratio are similar to those found in references 3 and 4 for the incompressible flow version of the code.

A more stringent restriction on the range of delta wing aspect ratios for which the code may be successfully utilized is illustrated in figures 32 and 33. These figures have been prepared with the help of Mr. Jim Luckring and Dr. Sudhir Mehotra at the NASA/Langley Research Center. These figures show the variation of theoretical lift coefficient for delta wings with aspect ratio at fixed angles of attack of 15° and 20° respectively. Solutions are for M = 0, and have converged so that the sum of the squared residuals is of the order 10^{-3} or less. These results for 30 and 42 wing panels are compared with the suction analogy which is known to be a good estimator of the actual C_L (reference 10). The separated flow theory grossly overpredicts C_L at the higher aspect ratios. This trend is stronger at the lower angle of attack. Also, the separated flow theory underpredicts C_L at the lower aspect ratios. Reasonable agreement between the suction analogy and the free vortex sheet theory at these angles of attack is judged to occur in the range of aspect ratios of $0.5 \leq A \leq 1.5$.

This disagreement between the current code and the suction analogy at higher and lower aspect ratios was not observed in the earlier version of the code. In reference 4 results for this incompressible flow code for an A = 2.0 flat delta wing are shown to agree well with both the suction analogy and experimental data. It is believed that the current treatment of the force-free boundary condition may be the source of these inconsistent results at aspect ratios above 1.5. Currently, the fed sheet termination of the shed vortex system has a force-free boundary condition applied on each fed sheet panel in a y-z plane, rather than in a direction normal to the individual panel. This approximation of the true boundary condition will be less accurate as the leading edge sweep is decreased.

Although converged theoretical results that are in general agreement with experimental data have been obtained for a cambered wing, as detailed in the previous section of this report, it must be emphasized that more generally cambered wings have not been found to converge. In particular, an apex cambered A = 1.147 delta wing has been investigated in detail. Details of this wing geometry and experimental force and pressure data are presented in references 14 and 15. Approximately 25 different computer runs for this planform were attempted with various wing paneling schemes, paneling densities, angles of attack, and shed vortex system initial locations. It was not found possible to reduce the initial solution squared residuals below four, and these residuals did not decrease with increasing iterations. It is believed that generally cambered and twisted wing configurations cannot be successfully modeled using the current code, due to the least squares character of the quadratic doublet distributions on each panel. Doublet sheet strengths may have jumps at panel edges, and if any panel control points come sufficiently close to these panel edges, the solution accuracy is degraded. This is particularly unfortunate since it is through use of control points near panel edges that matching of the various networks is achieved. These discontinuities in doublet strength may also be

caused by the near-plane approximation used to form each flat elemental panel in a network.

Another related program limitation is the inability to handle a streamwise wing tip. This is also believed to be a limitation of the six degree of freedom spline doublet distribution used in the theory, where the wing panel at the wing tip and trailing edge does not have a sufficient number of degrees of freedom to enable it to satisfy all of the required boundary conditions.

As seen in the previous section, the theoretical results are somewhat dependent upon the wing paneling arrangement. All numerical C_L results presented in figures 32 and 33 display a variation of lift coefficient for delta wing configurations with between 30 and 42 wing panels. Although no general criterion has been found for a minimum number of wing panels needed to obtain good agreement with experimental results, it has generally been found helpful to use unequally spaced panels, with smaller panels near the wing leading and trailing edges.

Two final problem areas relate to the adequacy of the model of the separated spiral vortex system. In all configurations it is required that the user specify what portions of the wing flow field are separated and what remain attached. At times this information may not be available. Second, there is a need for a more flexible starting solution for the initial guess of the location of the separated vortex system. Currently, a conical flow solution is used to initially locate the vortex. This has been found to be adequate for most planar wings, but not for three-dimensional cambered wings.

Since input data preparation was tedious for general three-dimensional wing configurations, a modified input format was developed as detailed in the Appendix. This modified input format allows the specification of either a single wing mean line shape, or varying camber and twist with span station. The Appendix gives detailed user instructions and presents sample input data.

CONCLUSIONS

It has been found that the separated flow program under development by the Boeing Commercial Airplane Company adequately predicts wing forces and pressure distributions for a series of thin, sharp-edged wings of delta, diamond, arrow, and double-delta planform for Mach numbers below 0.8, angles of attack between 10° and 30°, and aspect ratios between 0.5 and 1.5. Cambered wings cannot, in general, be modeled successfully. Conically cambered wings can be modeled, including the conically cambered delta experimentally investigated by Wentz and the circular arc spanwise camber wings of Barsby.

To extend the range of usefulness of the current theory it is recommended that:

(1) The current fed sheet force-free boundary condition be reexamined;

(2) A better technique be developed for obtaining an initial shape of the shed vortex sheet; and

(3) The possibility of implementating a more sophisticated panel type be investigated.

Blank Page

APPENDIX

BOEING PROGRAM MODIFICATION DOCUMENTATION AND USAGE INSTRUCTIONS

Blank Page

BOEING PROGRAM MODIFICATION DOCUMENTATION AND USAGE INSTRUCTIONS

A simplified input format has been developed for the generation of three-dimensional networks for use in the Boeing separated flow pilot code. These program modifications generate the desired, interpolated elevations for a cambered, twisted thin wing for wings whose leading and trailing edges are comprised of a finite number of straight line segments. The original code is utilized to generate the wing plan view (that is the x,y coordinates). The modified code can handle wings with a single equation describing the mean line for all span stations or wings with varying camber and twist with the spanwise direction. Also, input modifications have been developed to generate the mean surface for conically cambered delta wings of two types: 1. circular arc spanwise camber (Barsby, ref. 17), and 2. the conically cambered delta investigated by Wentz (ref. 14).

INPUT DATA PREPARATION

A deck must first be prepared to generate the desired networks for the flat plate representation of the configuration to be studied. The wing plan view itself will be generated either through use of the $ QUADRILATERAL preprocessor or the $ GOTHIC preprocessor.

The three-dimensional character of the wing is determined by use of the new modifications which utilize the $ CAMBERED WING preprocessor. This preprocessor generates the z coordinates for the (x,y) coordinates of the flat wing representation of the desired 3-D wing through interpolation. In general, the cambered surface is defined through a set of input data specifying the wing mean lines in the chordwise direction at a limited number of spanwise stations (no more than 24). It is also possible to input a fixed mean line shape valid for all span stations scaled to the local chord. The $ CAMBERED WING

preprocessor also can be used to generate the camber surface for wings with spanwise camber.

Thus, the current technique for generation of three-dimensional wing networks consists of two steps:

(1) Generate wing plan view, with desired paneling density using $ GOTHIC or $ QUADRILATERAL.

(2) Generate wing z coordinates using $ CAMBERED WING.

A description of the input card preparation, following the $ GOTHIC or $ QUADRILATERAL input cards is as follows (data are input in 6F10.0 format):

Card	Column	Variable	Comment
1			$ CAMBERED WING
2	1-10	KN	Network number
3	1-20	NRJK, NCJK	Number of rows (spanwise) and number of columns (chordwise)*
4	1-20	CNTRL, CNTJK	(1) CNTRL controls which type of wing is generated: CNTRL = 1. generates a delta wing, CNTRL = 2. is for a general 3-D wing, CNTRL = 3. generates the Wentz conical cambered delta, and CNTRL = 4. generates the Barsby conical cambered deltas

* In inputing z's for the conical camber wings, the user must set NRJK = NROW, NCJK = NCOL.

Card	Column	Variable	Comment
4 (continued)			(2) CNTJK = 1 is for a single mean line for all span stations CNTJK = 2. is for varying camber and twist with span. (CNTJK is used only for CNTRL equal to 1 or 2).

The input cards hereafter differ and will be described for each of the 4 possible values of CNTRL, starting with the simplest case.

(1) If CNTRL = 3. a conically cambered delta wing will be generated where the first (0.805) b/2 is flat and at the maximum z, and the remainder of the wing semispan is a portion of a circular arc. The maximum z is 0.105 of the wing local semispan. See references 14 and 15 for a description of these wings. When CNTRL = 3., no further data cards are required.

(2) If CNTRL = 4., a conically cambered delta wing will be generated, where the wing is a portion of a circular arc in the spanwise direction determined by the equation (see reference 17):

$$z_{local} = \frac{(b/2)_{local}}{2p} \left\{ \sqrt{(1 + p^2)^2 - \left(\frac{2p\, y_{local}}{(b/2)_{local}} \right)^2} - \sqrt{(1 + p^2)^2 - (2p)^2} \right\}$$

where p = 0.0 corresponds to a flat wing and p = 1.0 corresponds to a wing which is one half of a cone. One further data card is then required to specify the value of p.

Card	Column	Variable	Comment
5.	1-10	P1	$0.0 \leq p \leq 1.0$

(3) If CNTRL = 2.0 a three-dimensional general wing will be generated. The input cards needed depend on whether or not the camber shape varies with the spanwise direction.

a. If, when CNTRL = 2.0, CNTJK = 1.0, a 3-D wing with a single camber shape will be generated. The necessary input cards are as follows:

Card	Column	Variable	Comment
5.	1-60	XLE(I), I = 1, NRJK	These x values of the wing leading edge must be consistent with the wing planform generated using $ GOTHIC or $ QUADRILATERAL
6.	1-60	YLE(I), I = 1, NRJK	same as above; these are the y-values of the leading edge cuts at which the x's and chords are specified.
7.	1-60	CLOC(I), I = 1, NRJK	CLOC(I) is the wing local chord at y = YLE(I)
8.	1-60	PCTX(I), I = 1, NCJK	PCTX(I) is a table of percent local chord at which the z percent local chord is to be specified on the following card.

Card	Column	Variable	Comment
9.	1-60	PCTZ(I), I = 1, NCJK	PCTZ(I) is a table of the z values in percent local chord.

This completes the necessary input for a general wing with a single mean line shape. The desired z values for the paneling generated in ∯ GOTHIC or ∯ QUADRILATERAL are then found through linear interpolation.

b. If when CNTRL = 2.0, CNTJK = 2.0, a 3-D wing with camber and twist varying with span station will be generated. (Note that as previously mentioned, when CNTRL = 2.0, it is not necessary to specify NRJK = NROW for the network in question or NCJK = NCOL. The only restrictions are NRJK, NCJK $\leq$ 24). The necessary input cards are

Card	Column	Variable	Comment
5.	1-60	XLE(I), I = 1, NRJK	see previous card 5
6.	1-60	YLE(I), I = 1, NRJK	see previous card 6
7.	1-60	CLOC(I), I = 1, NRJK	see previous card 7
8.	1-60	PCTX(I), I = 1, NCJK	see previous card 8
9.	1-60	(PCTZ(I), I = 1, NCJK) have NRJK cards, one for each span station	Note: Currently the code accepts the PCTZ values to be the actual, dimensional z values desired rather than the percent values.

(4) If CNTRL = 1.0, a 3-D delta wing is generated. This case is not described since it is a subset of the general case described above (CNTRL = 2.). These program mods are contained in a deck labeled *IDENT DIM3D.

FURTHER CONSIDERATIONS

Other minor program modifications have been made, including the following:

(1) The program can now be run with no shed vortex systems to check the accuracy of the code for attached flow. (Be sure to set # ITERATIONS equal to zero).

(2) The program now calculates the forces and moments on each network twice: once using the 2nd order C_p's, and once using the isentropic C_p's. It has been found, as claimed by Boeing, that use of the isentropic C_p's gives better aggrement with experiment than the second order C_p's in the separated flow case, but that these isentropic C_p's yield answers in the attached flow cases which differ from other attached flow methods such as reference 7 by as much as 18 percent, for Mach numbers other than zero. The two C_p's are identical at M = 0.

These two program mods are contained in a deck given the name *IDENT JMK.

(3) The program can, in an attempt to obtain a more reasonable starting solution than the conical flow solution now used, rotate such a shed sheet network to be locally perpendicular to the wing leading edge in a y-z plane. These program modifications are contained in a deck labeled *IDENT ROT. However, it has been found that better results are obtained when the vortex system is rotated through only a fraction of the droop angle.

Examples of two of the three possible modified input formats follow.

LIST OF INPUT DATA CARDS

Blank Page

```
$CASE
DELTA WING WITH SHED SHEETS. APEX CAMBERED SURFACE
CHECKOUT OF INTERPOLATION OF PANELLING AND ROTATION OF SHED SHEETS
$ANGLE OF ATTACK
20.
$YAW
0.
$SYMMETRY CODE
1.
$MACH NUMBER
0.0
$NETWORK  (GENERAL INPUT)
6.
$ROW
7.          9.          3.          2.          2.          2.
$COLUMN
8.          8.          8.          7.          9.          3.
$TYPE
2.          4.          14.         8.          8.          10.
$UPDATE INDICES
0.          4.          2.          0.          1.          1.
1.
1.          3.          4.
1.
2.          3.          4.
1.
2.          2.          2.
1.
3.          2.          2.
$QUADRILATERAL PREPROCESSOR
1.
0.0         0.0         0.0         30.0        0.0         0.0
30.0        8.62        0.0         0.0         0.0         0.0
7.
0.0         0.3         0.5         0.625       0.75        0.875
1.
8.
0.0         .15         .25         .35         .45         .6
.8          1.0
0.
$CAMBERED WING
1.
7.          8.
2.          1.
0.          3.48028     8.700696    13.921114   19.141531   24.36195
30.
0.          1.          2.5         4.          5.5         7.
8.62
30.         26.51972    21.299304   16.078886   10.858469   5.638051
```

Sample Case 1 - Apex cambered delta wing from reference 14 using CNTRL = 2.0, CNTJK = 1.0.

```
0.
0.          .075        .15         .3          .5          .7
.86666666 1.
0.          .024867     .030633     .025767     .0184       .011033
.004911     0.
$VORTEX PREPROCESSOR
2.          5.
8.
7.          14.         21.         28.         35.         42.
49.         56.
1500.
0.0
$TRAILING WAKE
4.
7.
50.         51.         52.         53.         54.         55.
56.
1500.
$REFERENCE
15.         0.          0.
129.3       1.          20.         1.
$ITERATION
1.
$PRINT
1.
$END OF CASE
0
```

```
$CASE
DELTA WING WITH SHED SHEETS, AND WITH CAMBERED SURFACE TO CHECK $CAM
CHECKOUT OF CONVERGENCE FOR CONICAL CAMBERED WINGS - WENTZ AND BARSBY
$ANGLE OF ATTACK
15.
$YAW
0.
$SYMMETRY CODE
1.
$MACH NUMBER
4.0
$NETWORK  (GENERAL INPUT)
6.
$ROW
10.        9.          3.          2.          2.          2.
$COLUMN
8.         8.          8.          10.         9.          3.
$TYPE
2.         4.          14.         8.          8.          10.
$UPDATE INDICES
0.         4.          2.          0.          1.          1.
1.
1.         3.          4.
1.
2.         3.          4.
1.
2.         2.          2.
1.
3.         2.          2.
$QUADRILATERAL PREPROCESSOR
1.
0.0        0.0         0.0         30.0        0.0         0.0
30.0       8.62        0.0         0.0         0.0         0.0
10.
0.0        0.3         0.5         0.7         0.805       0.85
.90        0.94        0.97        1.0
8.
0.0        .15         .30         .45         .60         .75
0.875      1.0
0.
$CAMBERED WING       CONICAL CAMBER  WENTZ  CR 2002
1.
10.        8.
3.         1.
$VORTEX PREPROCESSOR
2.         5.
8.
10.        20.         30.         40.         50.         60.
70.        80.
```

Sample Case 2 - Conical camber delta wing
from reference 14.

```
1500.
.15
$TRAILING WAKE
4.
10.
71.        72.        73.        74.        75.        76.
77.        78.        79.        80.
1500.
$REFERENCES
15.        0.         0.
129.3      1.         20.        1.
$ITERATION
6.
$PRINT
1.
$END OF CASE
0
```

REFERENCES

1. Brune, G. W.; J. A Weber; F. T. Johnson; P. Lu; and P. E. Rubbert: A three-dimensional solution of flows over wings with leading-edge vortex separation. Part I, Engineering Document. NASA CR-132709, September 1975.

2. Coleman, R. G.; F. T. Johnson and P. Lu: A three-dimensional solution of flows over wings with leading-edge vortex separation. Part II, Program Description Document. NASA CR-132710, September 1975.

3. Weber, J. A.; G. T. Brune; F. T. Johnson; P. Lu; and P. E. Rubbert: A three-dimensional solution of flows over wings with leading-edge vortex separation. AIAA Paper No. 75-866, presented at 8th Fluid and Plasma Dynamics Conference, Hartford, Connecticut, June 16-18, 1975.

4. Kuhlman, J. M.: Load distributions on slender delta wings having vortex flow. AIAA Journal of Aircraft, Vol. 14, No. 7, July 1977.

5. Stahl, W.; K. Hartmann; and W. Schneider: Force and pressure measurements on a slender delta wing at transonic speeds and varying Reynolds numbers, presented at AGARD meeting on facilities and techniques for aerodynamic testing at transonic speeds and high Reynolds numbers, Göttingen, April 26-28, 1971.

6. Stahl, W.; K. Hartmann; and W. Schneider: Aerodynamische Untersuchungen and Flugkörpern mit Flügeln Kleiner Streckug. Teil I: Kraft und Druckverteilungsmessungen an einem schlanken Deltaflügel in Unterschall-und transsonischer Stromung, Aerodynamische Versuchsanstalt Göttingen report 70 A 53, September 1971.

7. Margason, R. J.; and J. E. Lamar: Vortex lattice Fortran program for estimating subsonic aerodynamic characteristics of complex planforms. NASA TN D-6142, February 1971.

8. Lamar, J. E.; and B. B. Gloss: Subsonic aerodynamic characteristics of interacting lifting surfaces with separated flow around sharp-edges predicted by a vortex-lattice method, NASA TN D-7921, September 1975.

9. Polhamus, E. C.: A concept of the vortex-lift of sharp-edge delta wings based on a leading-edge-suction analogy. NASA TN D-3767, December 1966.

10. Polhamus, E. C.: Predictions of vortex-lift characteristics based on a leading-edge-suction analogy. AIAA Paper No. 69-1133, presented at AIAA 6th Annual Meeting, Anaheim, California, October 20-24, 1969.

11. Wentz, W. H., Jr.: Wind tunnel investigations of vortex breakdown on slender sharp-edged wings. NASA CR-98737, 1968.

12. Lamar, J. E.: Some recent applications of the suction analogy to vortex lift estimates. NASA SP-347, Aerodynamics Analyses Requiring Advanced Computers. March 1975.

13. Lamar, J. E.: Strake-wing analysis and design. AIAA Paper No. 78-1201, presented at the AIAA 11th Fluid and Plasma Dynamics Conference, Seattle, Washington, July 10-12, 1978.

14. Wentz, W.H., Jr.: Effects of leading-edge camber on low-speed characteristics of slender delta wings. NASA CR-2002, October 1972.

15. Wentz, W.H., Jr.: Effects of leading edge camber on low-speed characteristics of slender delta wings - techniques and tabulated data. NASA CR-112016, 1972.

16. Lamar, J. E.: Subsonic vortex-flow design study for slender wings. AIAA Paper No. 78-154, presented at the AIAA 16th Aerospace Sciences Meeting, Huntsville, Alabama, January 16-18, 1978.

17. Barsby, J. E.: Flow Past conically-cambered slender delta wings with leading-edge separation. ARC Reports and Memoranda No. 3748 September 1972.

Table 1. Tabulation of wing configurations modeled using separated flow theory.

		Mach Number	Angle of Attack	Converged?
1.	Flat delta wing, A = 0.52	0.0 - 0.8	10° - 30°	yes
2.	Flat delta wing, A = 0.705	0.0 ; 0.6	20°	yes
3.	Flat delta wing, A = 1.0	0.0	15° - 20°	yes
4.	Flat delta wing, A = 1.147	0.0	20°	yes
5.	Flat delta wing, A = 1.456	0.0	10° - 20°	yes
6.	Flat delta wing, A = 1.5	0.0	20°	yes
7.	Flat delta wing, A = 2.0	0.0	10° - 20°	yes
8.	Flat delta wing, A = 2.5	0.0	15° , 20°	no
9.	Flat delta wing, A = 4.0	0.0	20°	no
10.	70° Flat diamond wing	0.0	10° - 30°	yes
11.	70° Flat arrow wing	0.0	10° - 30°	yes
12.	80°/65° Flat double delta wing	0.0	5° - 30°	yes
13.	60° Flat cropped delta wing	0.0	20°	no
14.	72° Flat cropped delta wing	0.0	20°	no
15.	Flat delta wing, A = 1.147, attached flow (also in yaw)	0.0 - 0.6	10° - 30°	(no iteration required)
16.	Flat delta wing, A = 1.147, with thickness	0.0	20°	yes
17.	Flat delta wing, A = 1.147 in yaw; β = 10°	0.0	20°	yes
18.	80°/65° Flat double delta wing, with 2 shed sheet systems	0.0	20°	no
19.	A = 1.147 Conical cambered delta	0.0	10° - 30°	yes
20.	A = 1.147 Circular arc spanwise cambered delta	0.0	10° - 30°	yes
21.	A = 1.147 Apex cambered delta	0.0	10° - 20°	no
22.	Cambered, twisted arrow wing	0.0	20°	no

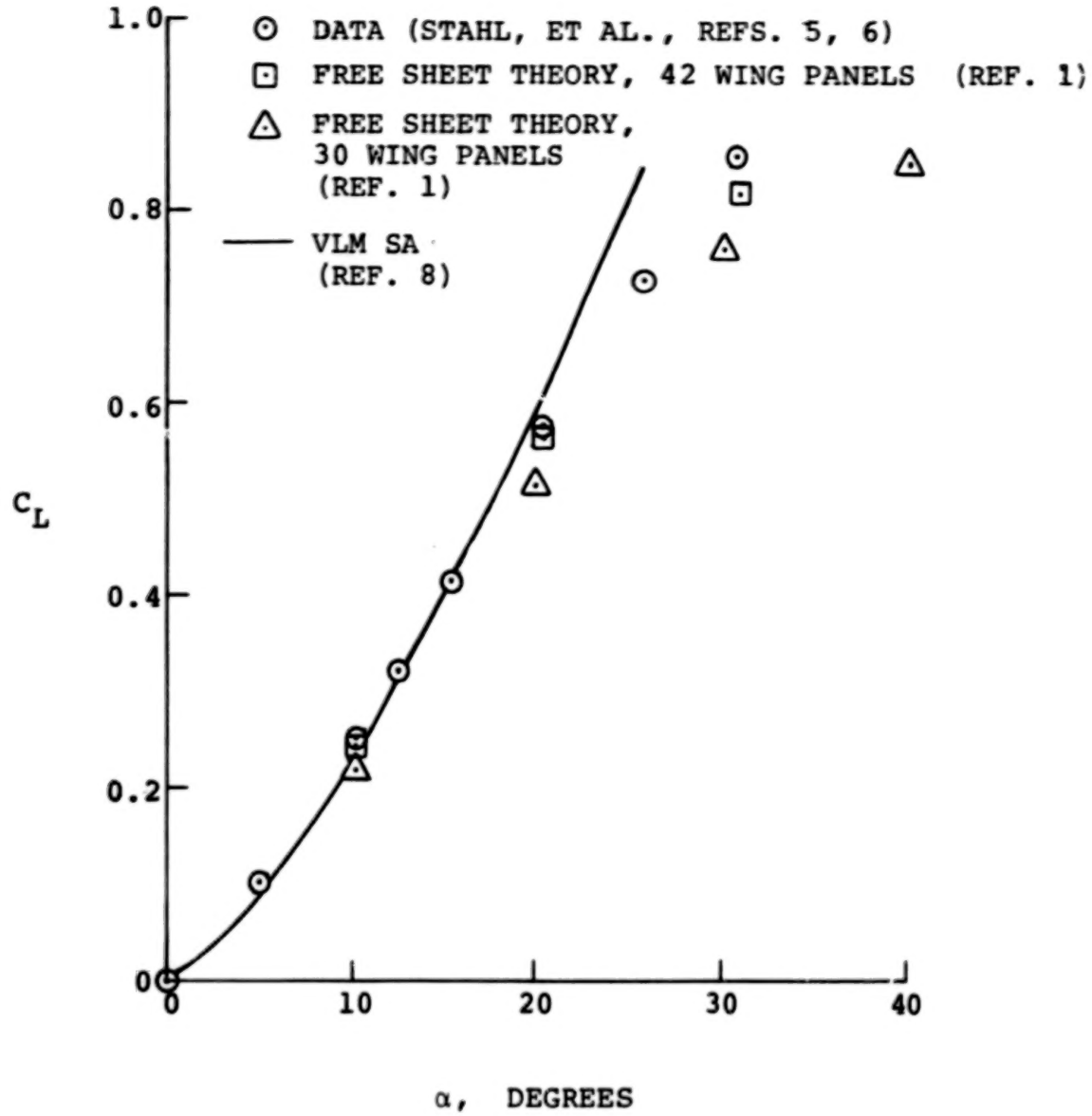

Figure 1. Lift coefficient comparison - A = 0.52 flat delta wing, M = 0.80.

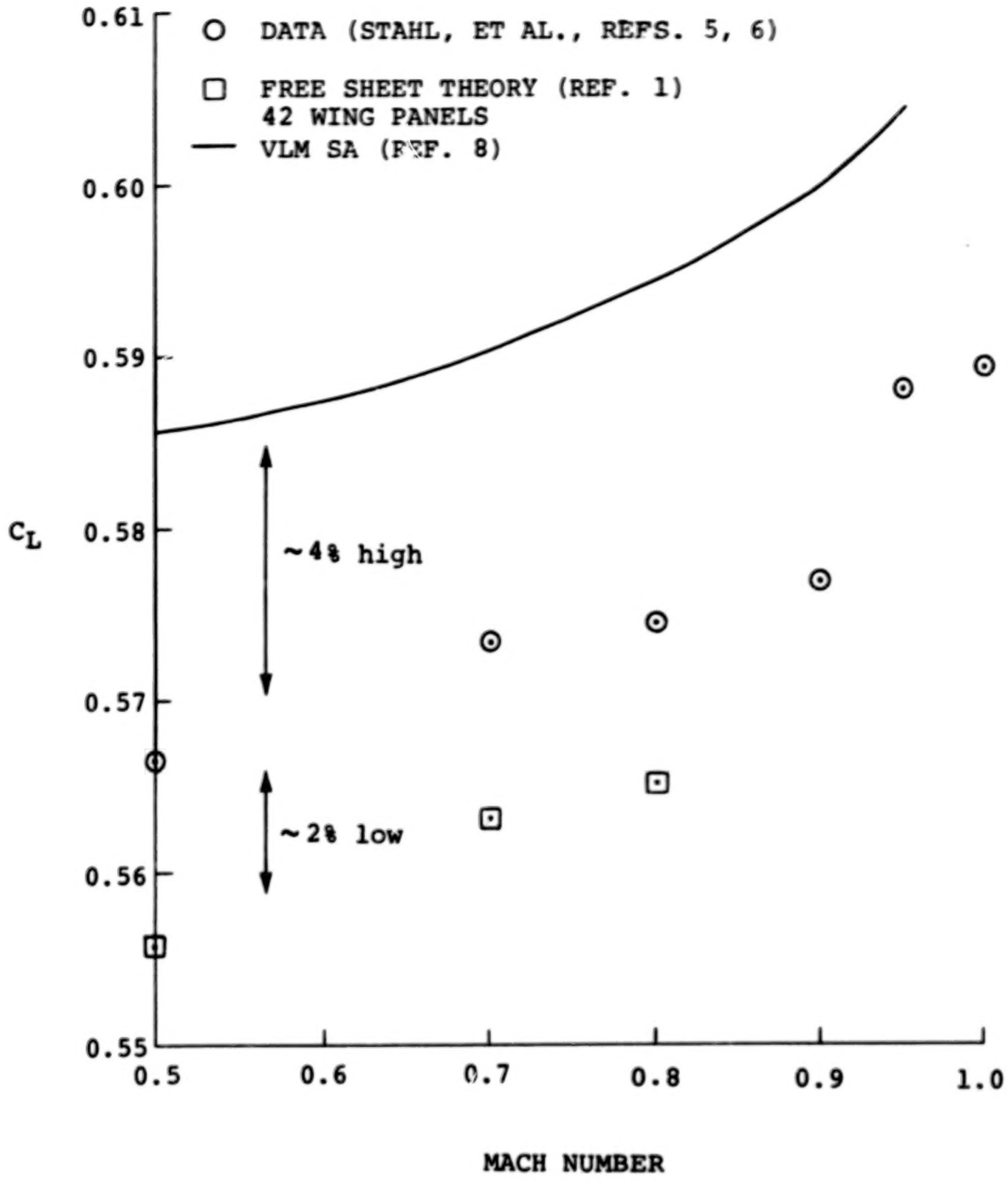

Figure 2. Lift coefficient dependence upon Mach number, for A = 0.52 flat delta, α = 20.8°.

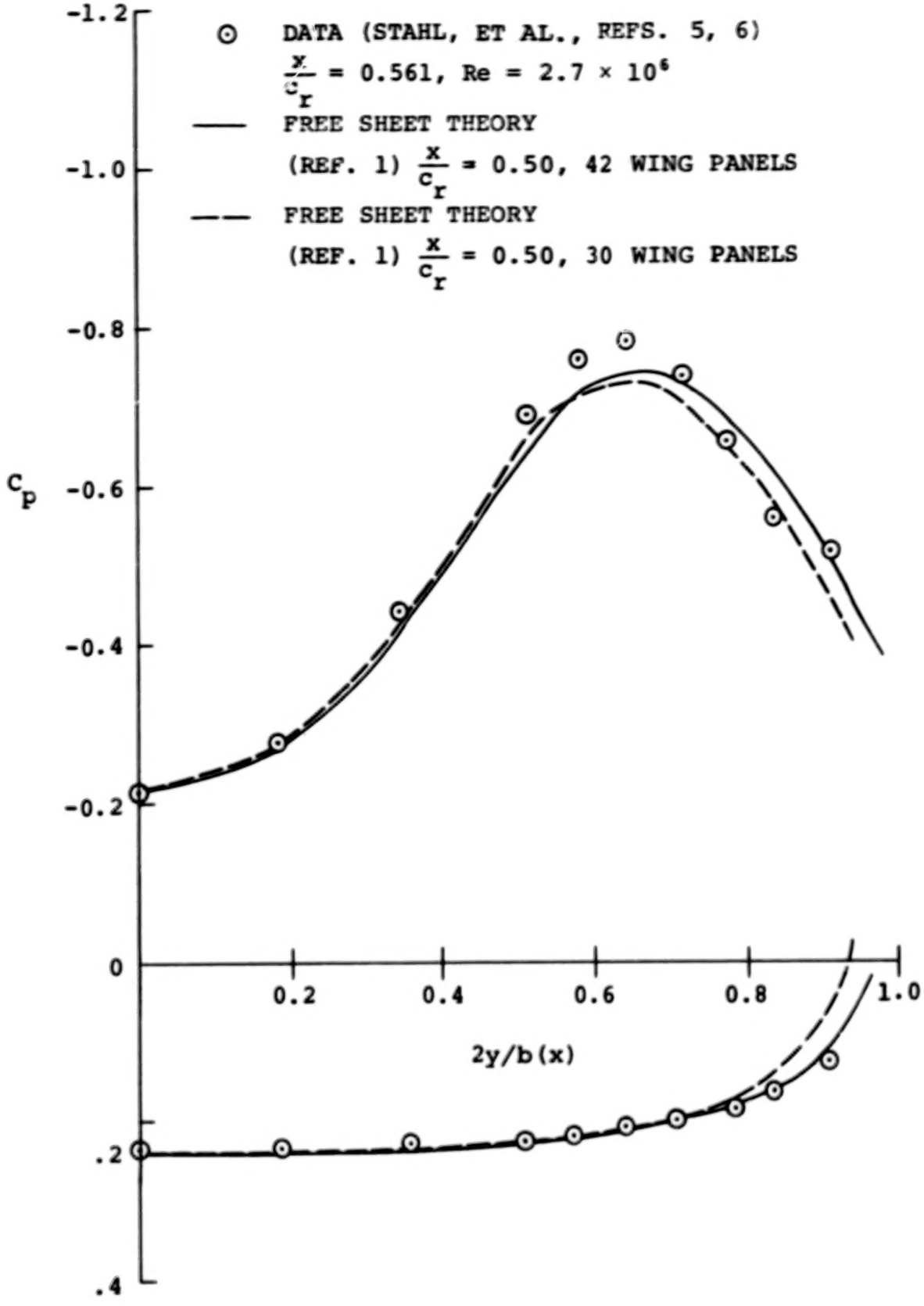

Figure 3. Pressure distribution for A = 0.52, M = 0.50, flat delta, $\alpha = 20.8°$.

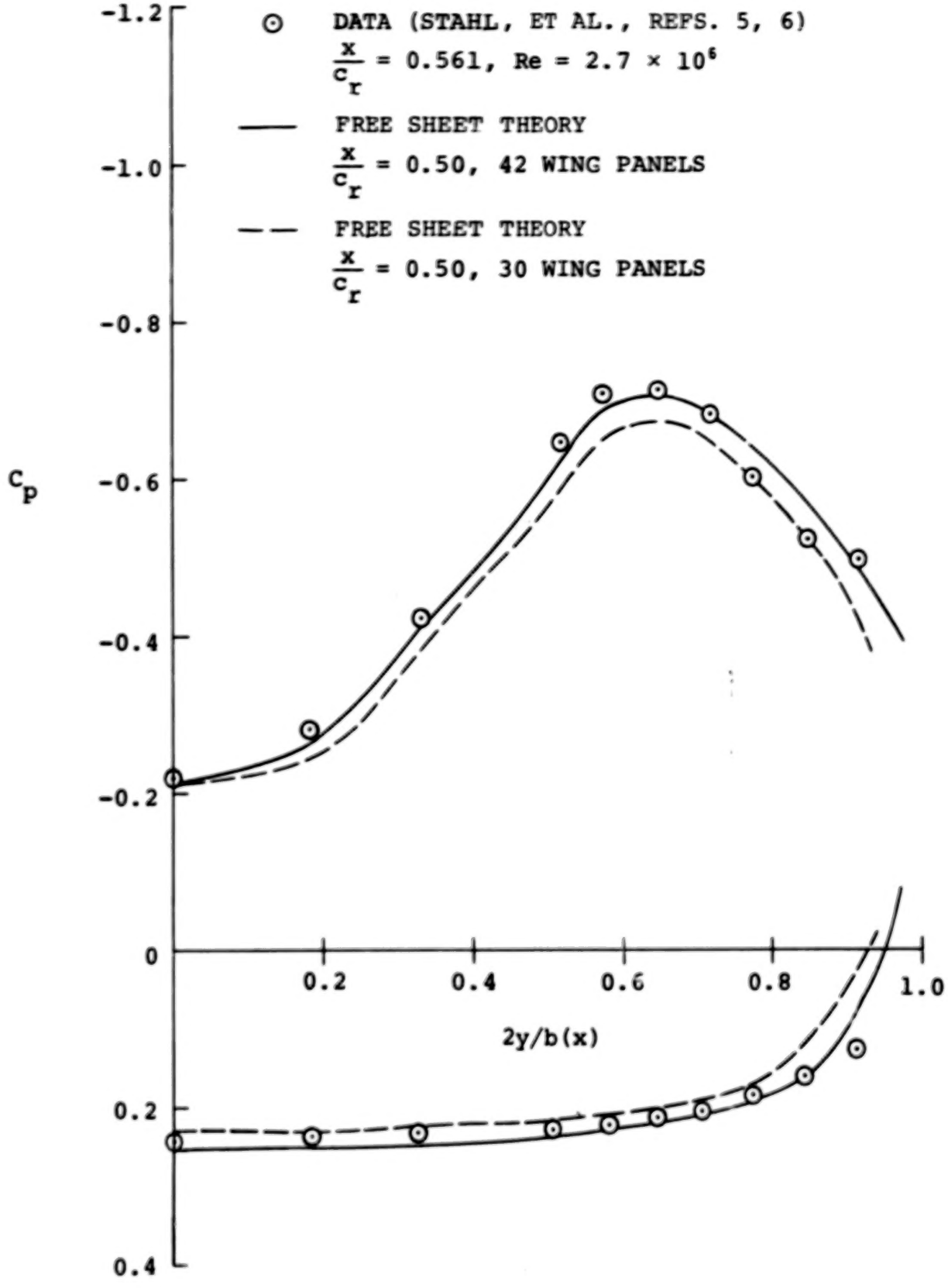

Figure 4. Pressure distribution for A = 0.52, M = 0.70, flat delta, α = 20.8°.

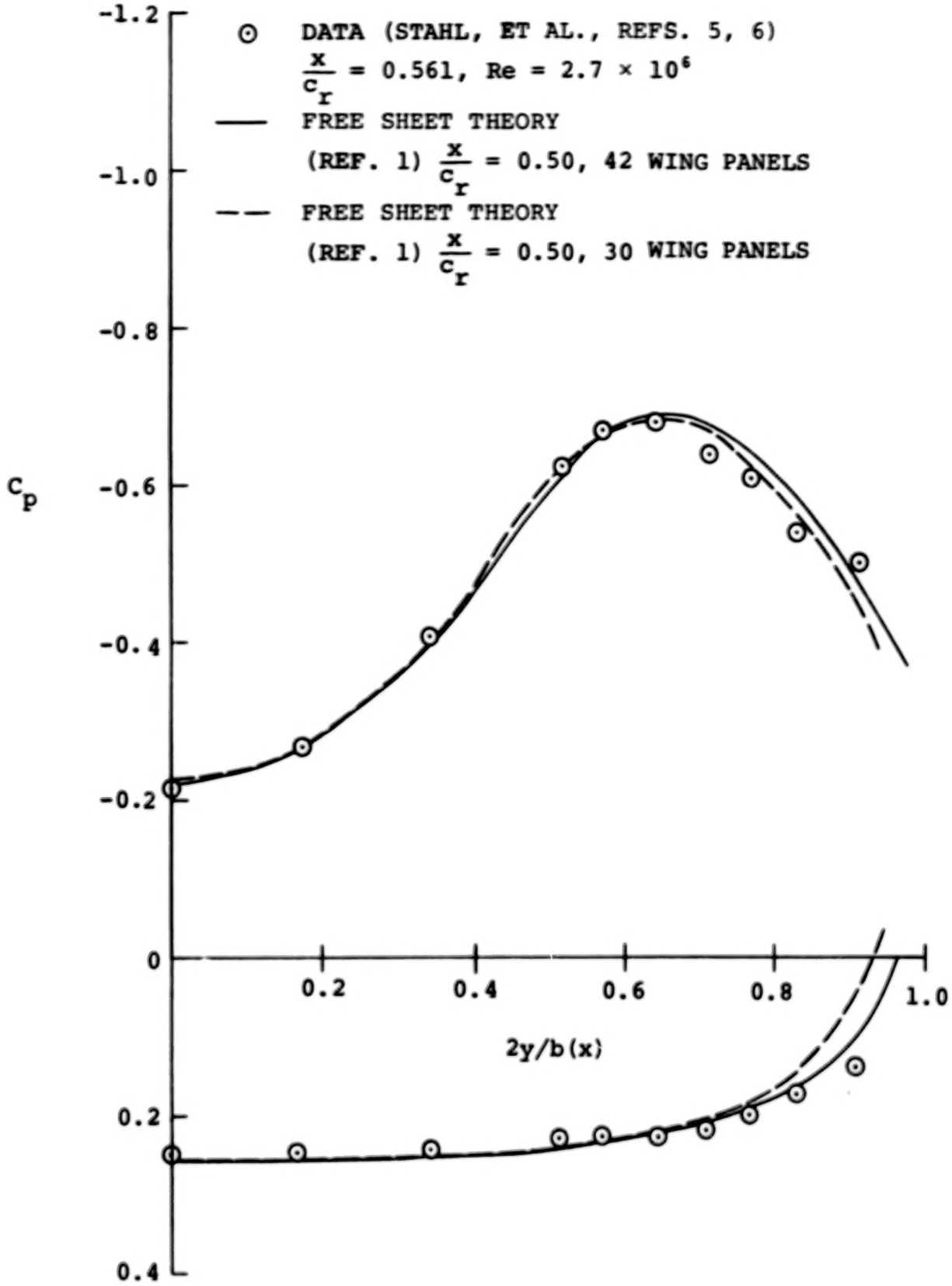

Figure 5. Pressure distribution for A = 0.52, M = 0.80 flat delta, α = 20.8°.

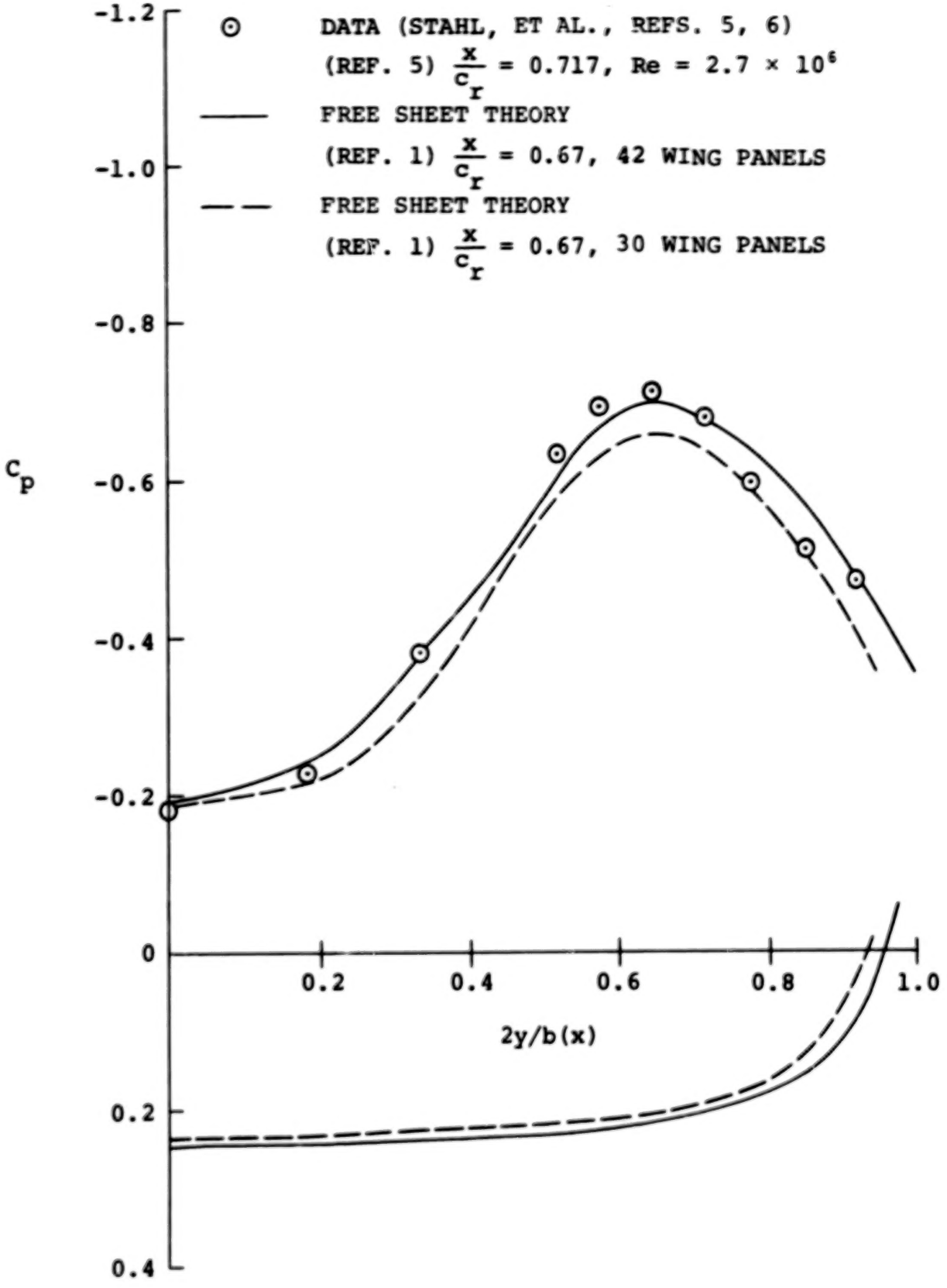

Figure 6. Pressure distribution for A = 0.52, M = 0.70 flat delta, $\alpha = 20.8°$.

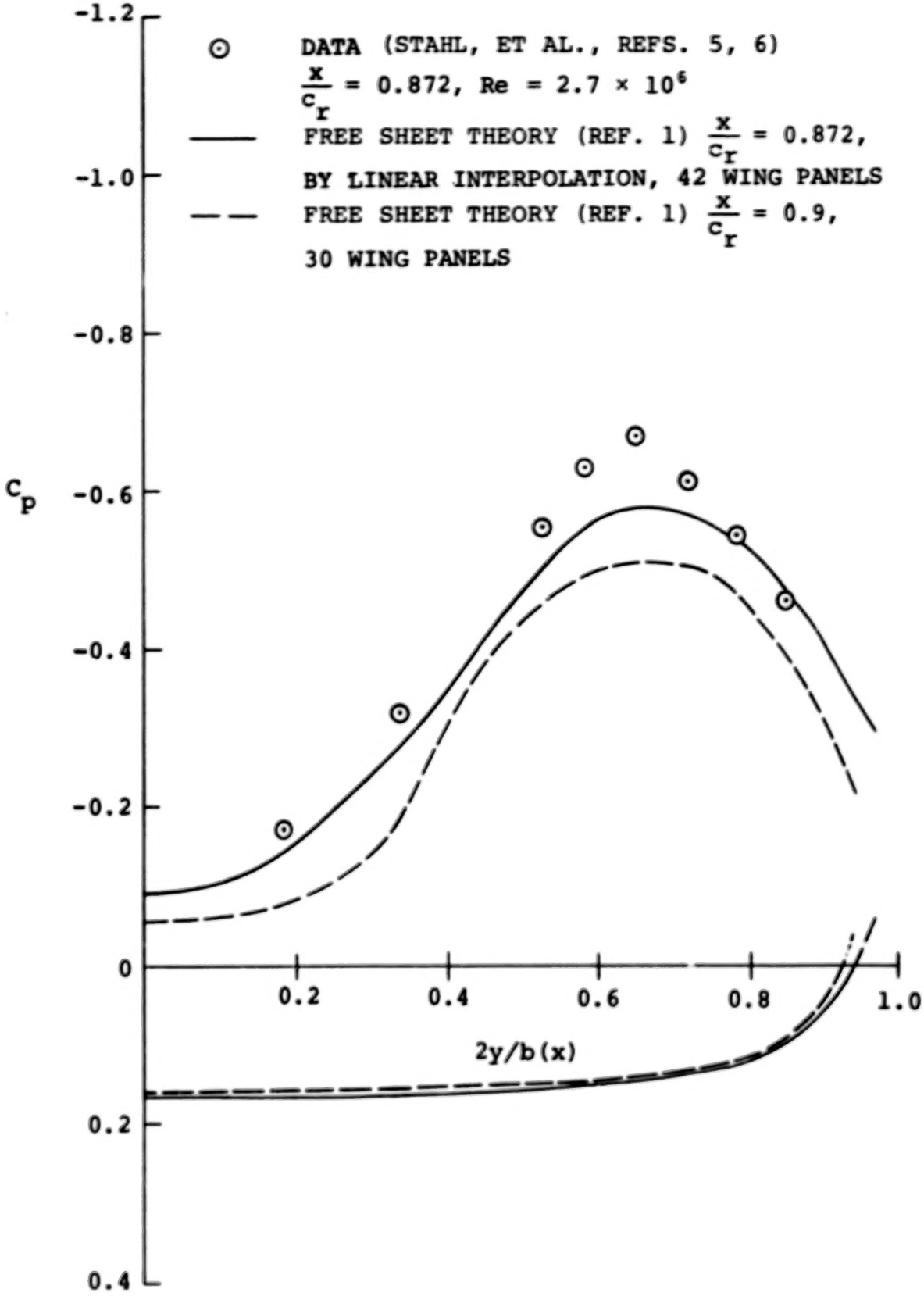

Figure 7. Pressure distribution for A = 0.52, M = 0.70, flat delta, α = 20.8°.

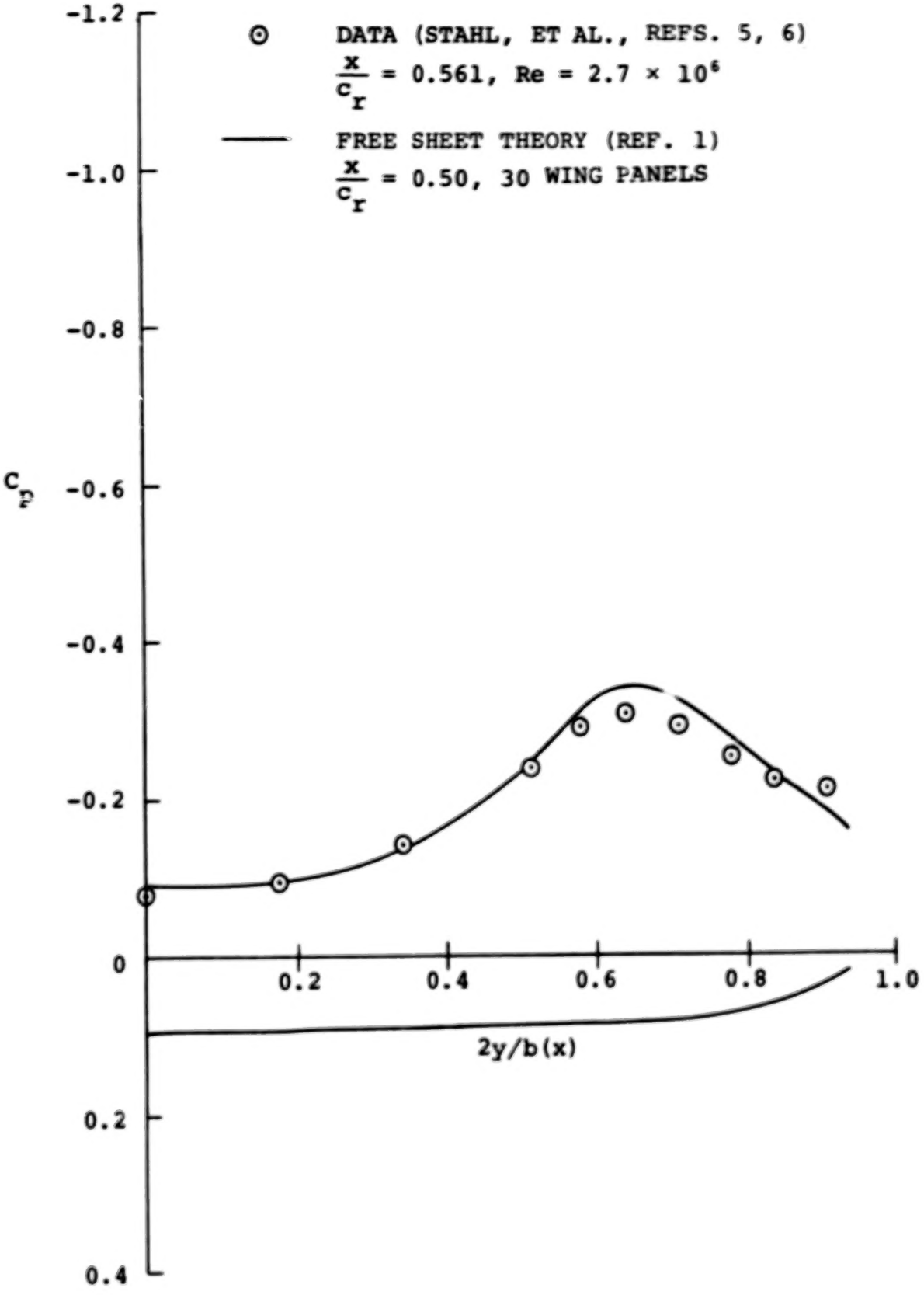

Figure 8. Pressure distribution for A = 0.52, M = 0.70, flat delta, α = 10.3°.

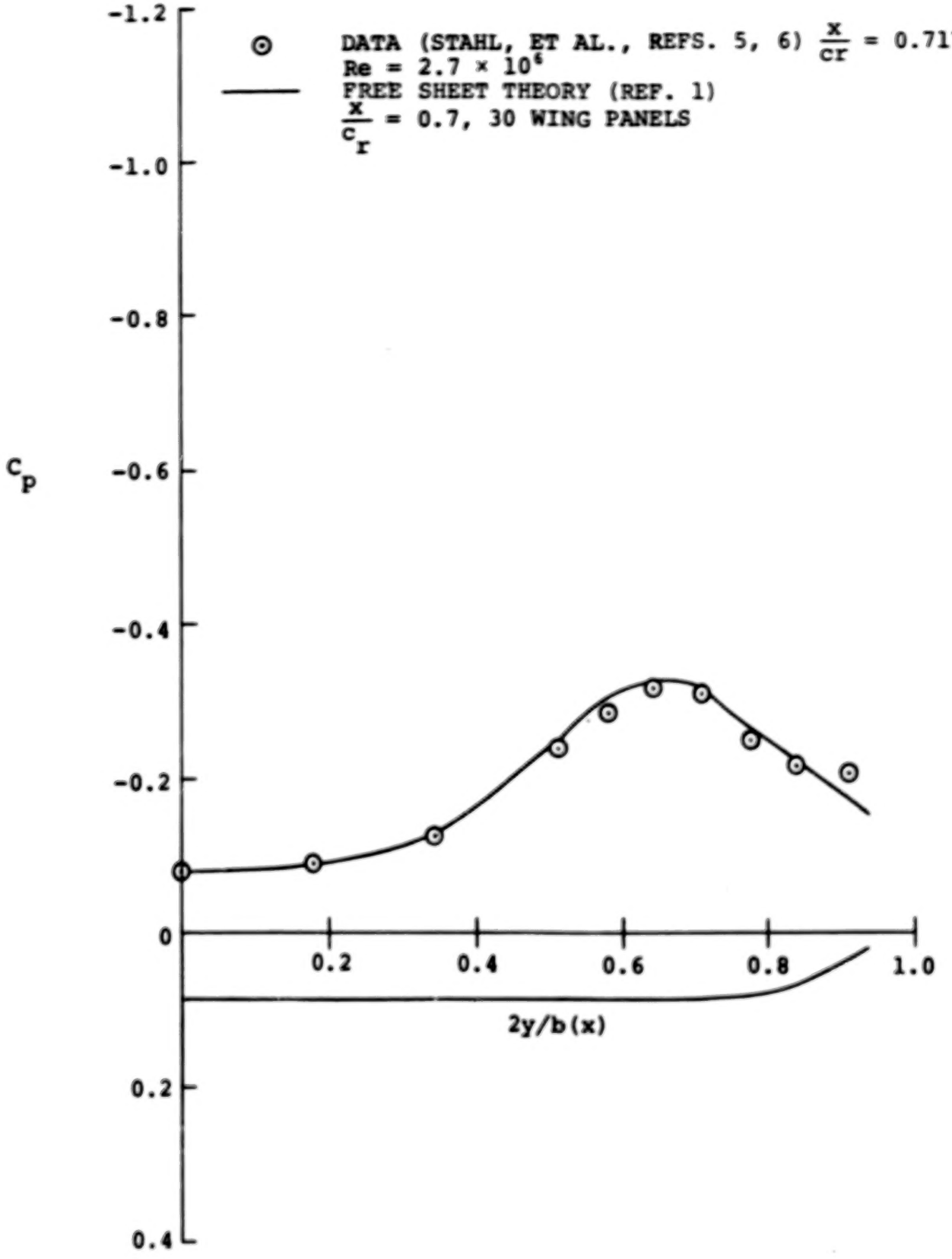

Figure 9. Pressure distribution for A = 0.52, M = 0.70, flat delta, α = 10.3°.

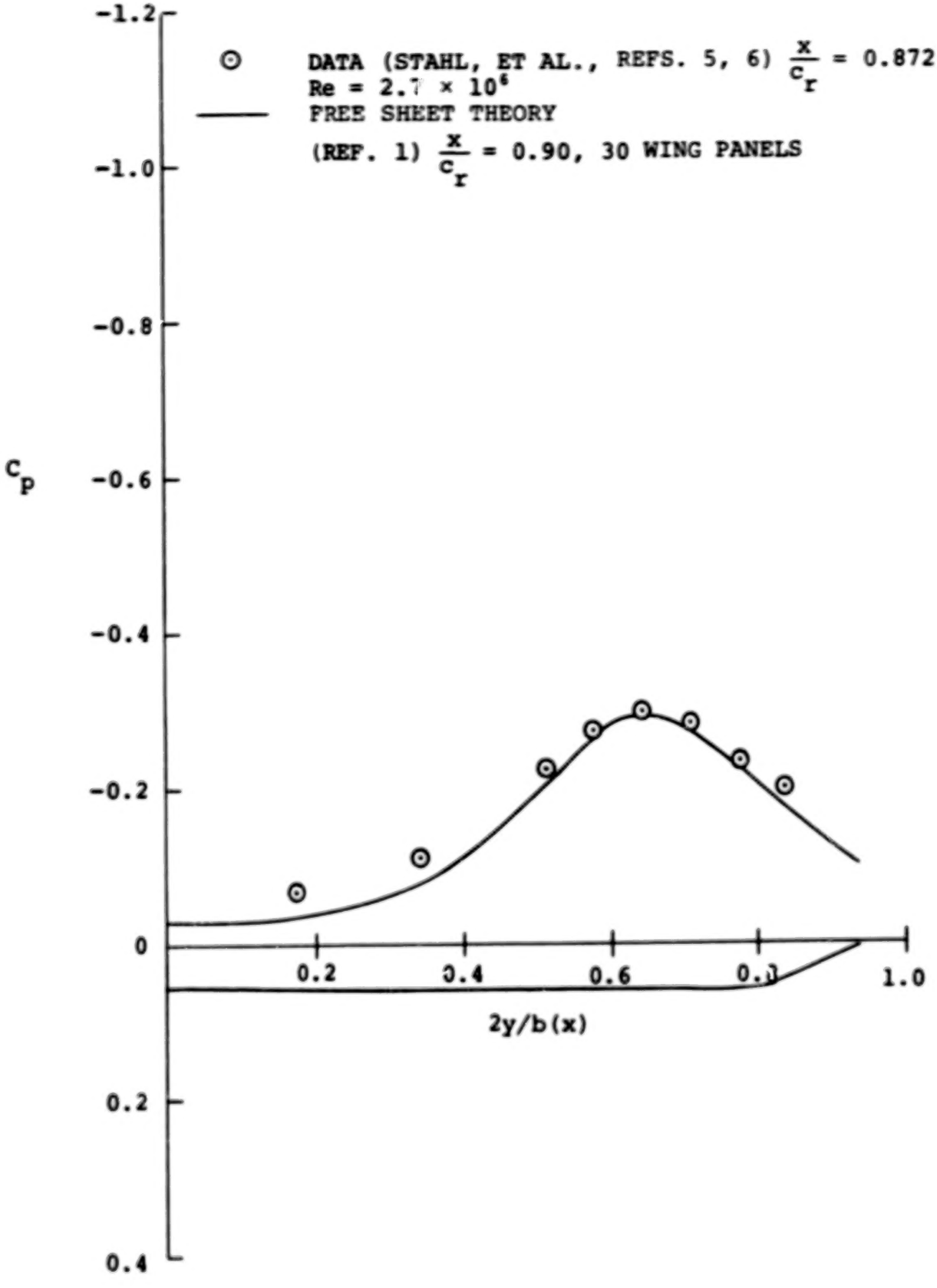

Figure 10. Pressure distribution for A = 0.52, M = 0.70, flat delta, α = 10.3°.

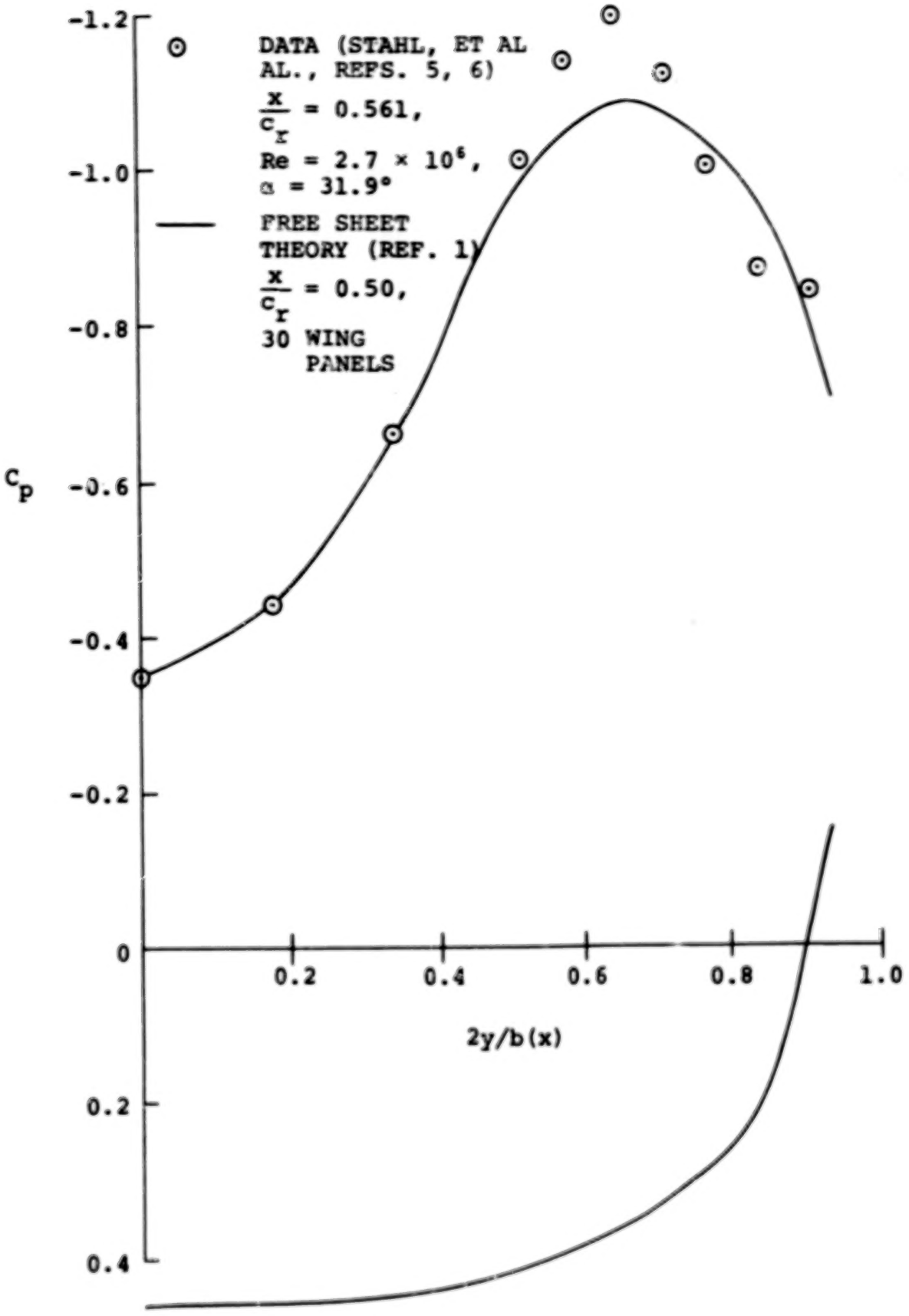

Figure 11. Pressure distribution for A = 0.52, M = 0.70, flat delta, $\alpha \cong 30°$.

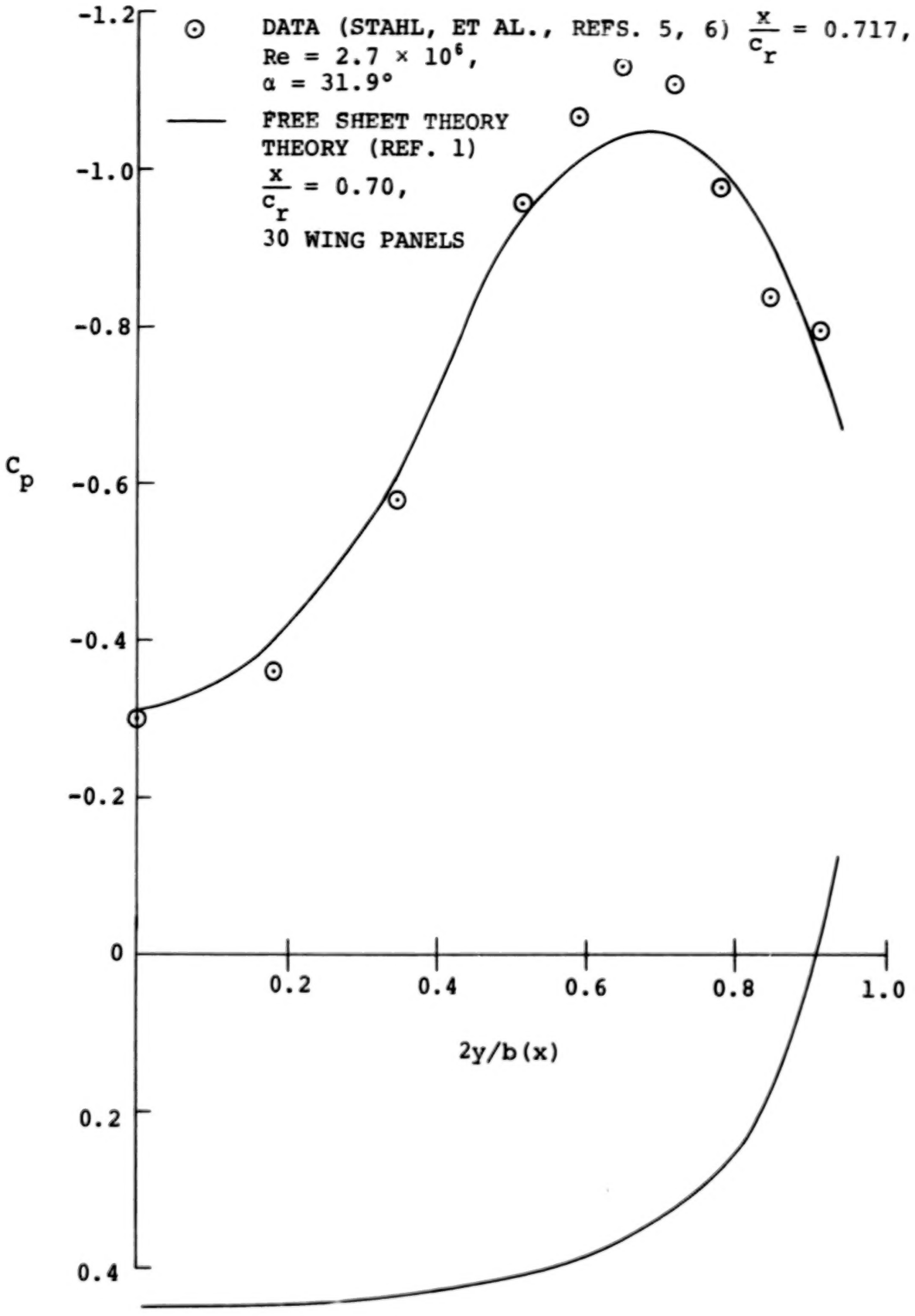

Figure 12. Pressure distribution for A = 0.52, M = 0.70 flat delta, $\alpha \cong 30°$.

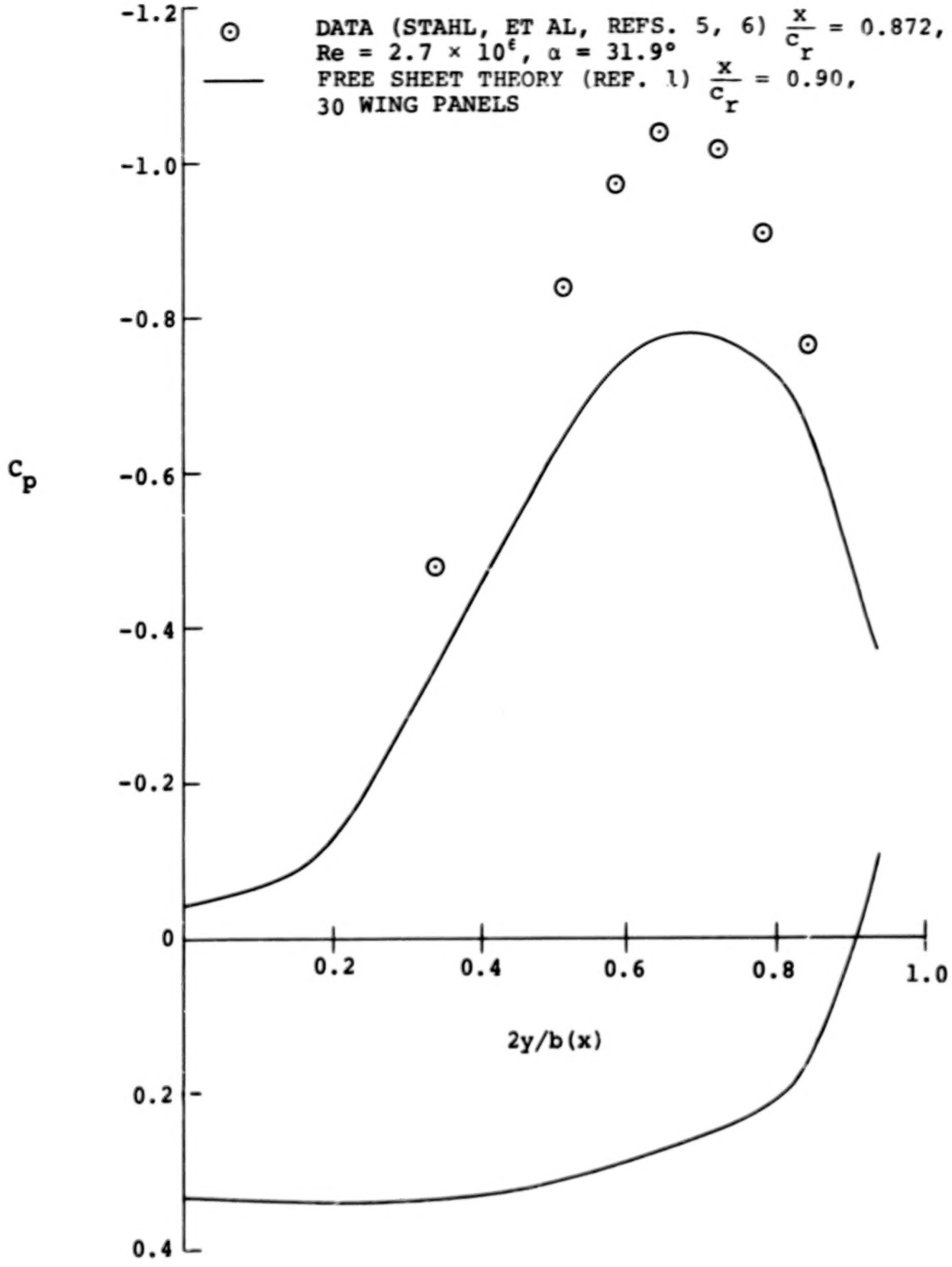

Figure 13. Pressure distribution for A = 0.52, M = 0.70, flat delta, $\alpha \cong 30°$.

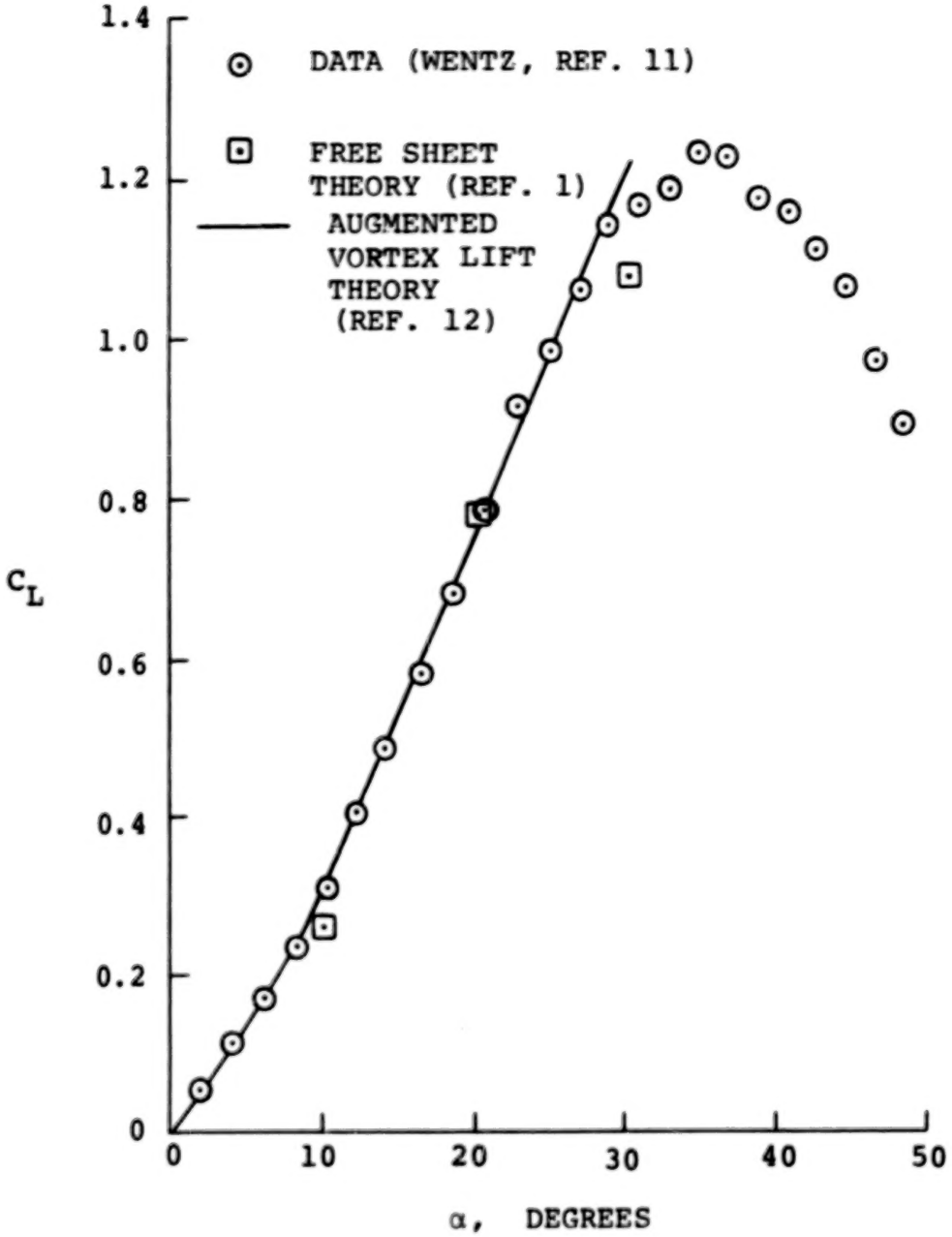

Figure 14. Lift coefficient comparison - 70° diamond wing, $M \cong 0$.

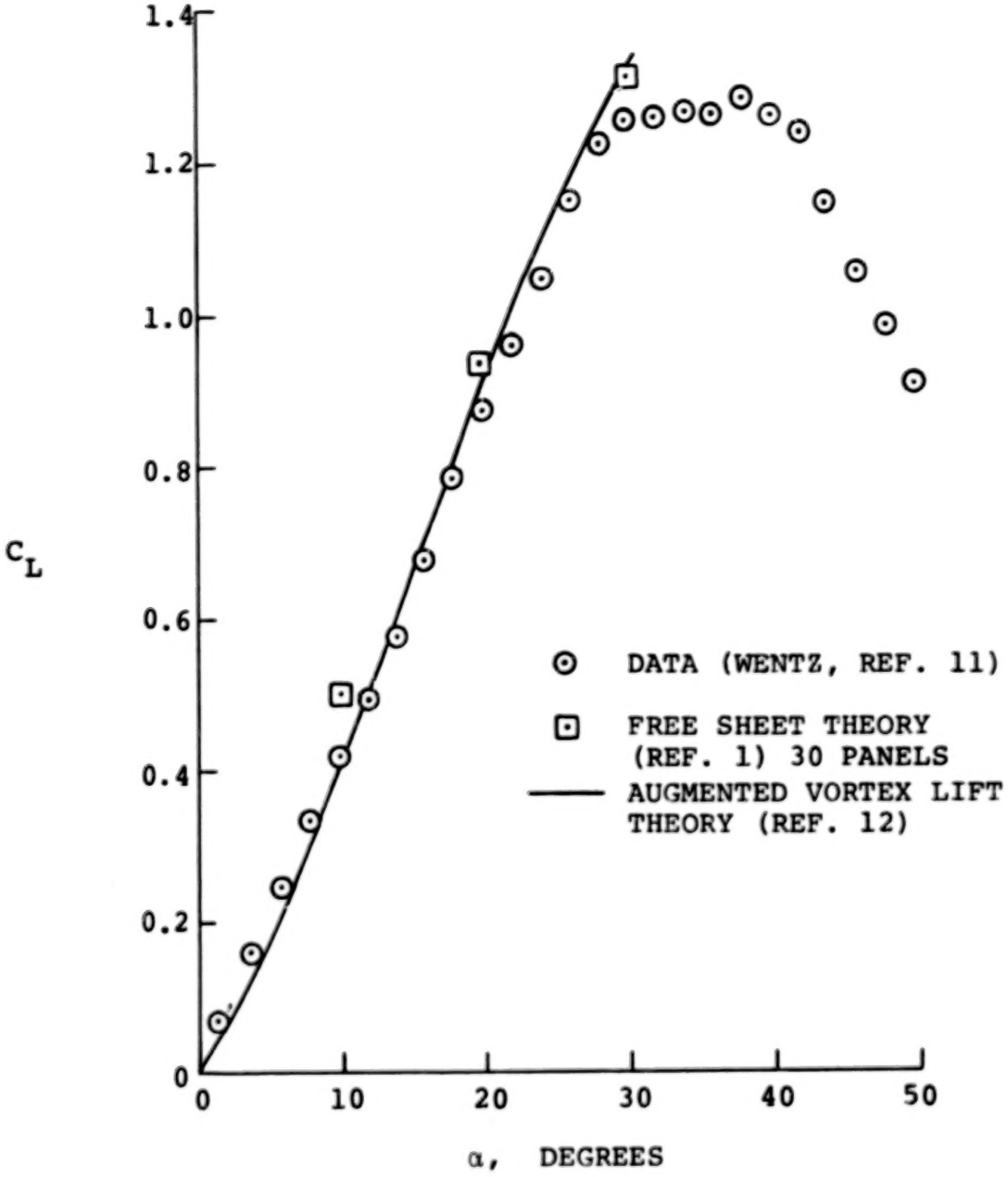

Figure 15. Lift coefficient comparison - 70° arrow wing, $M \cong 0$.

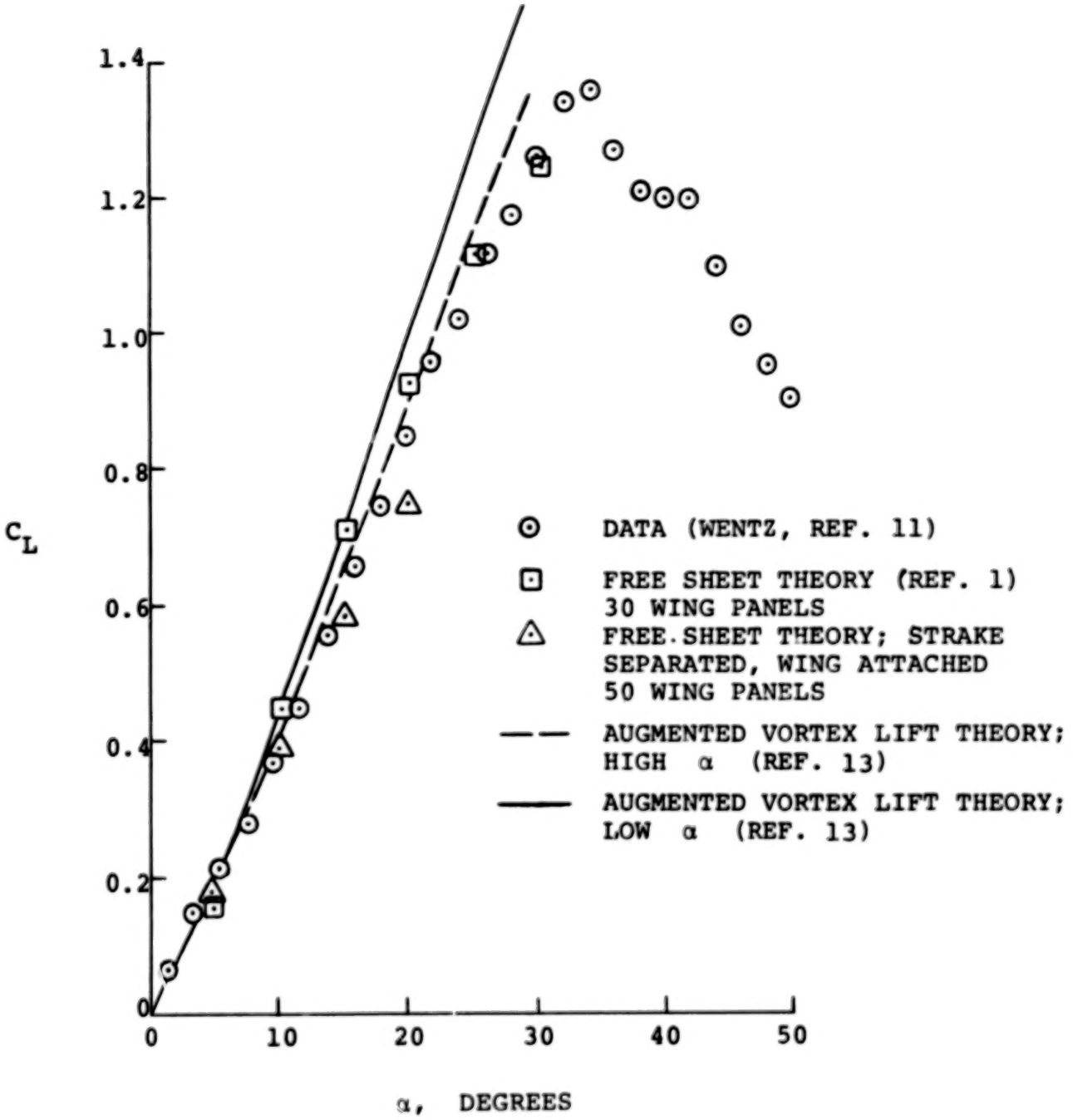

Figure 16. Lift coefficient comparison - 80°/65° double delta wing, M ≅ 0.

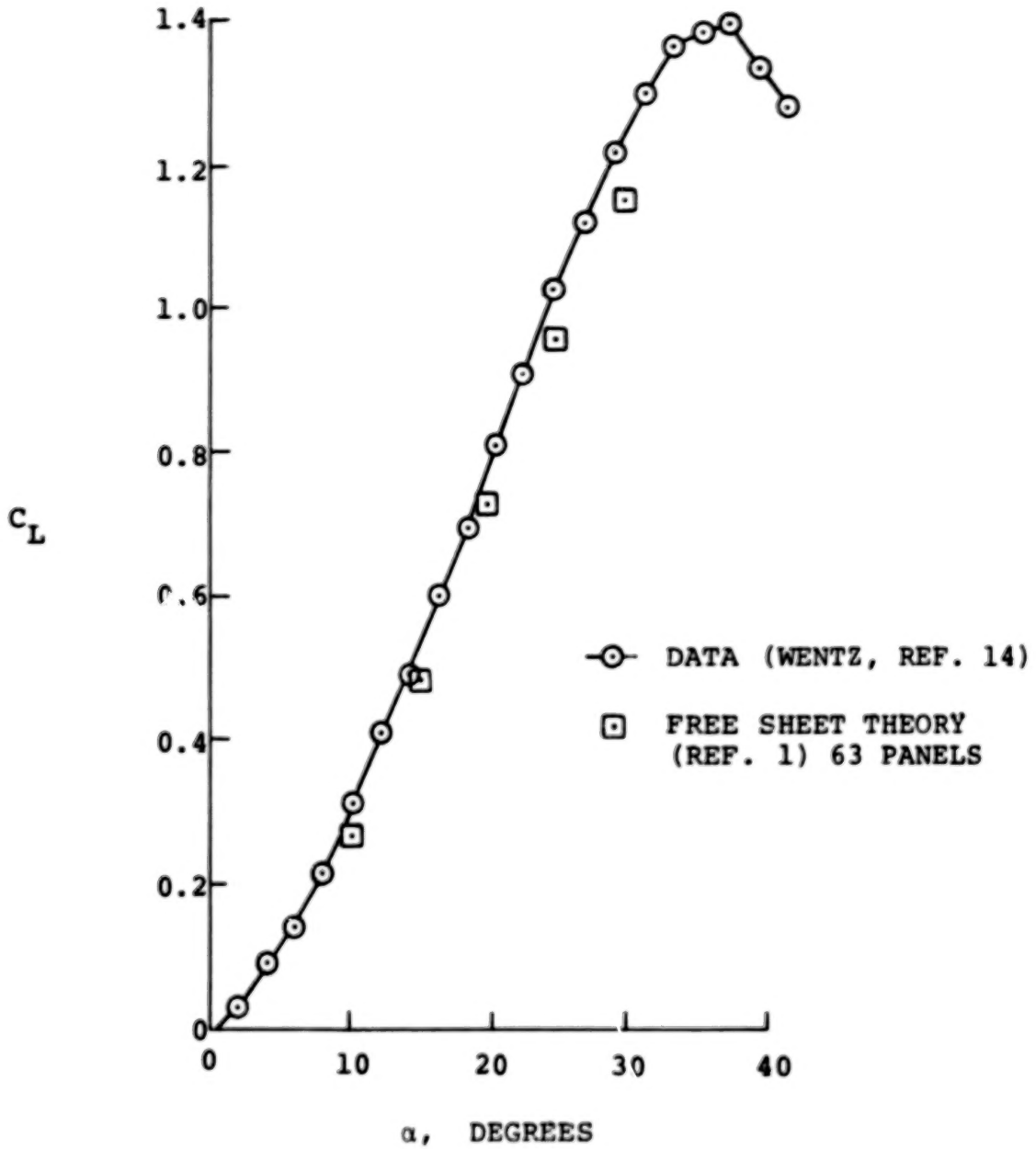

Figure 17. Lift coefficient comparison - conical camber delta, M ≅ 0.

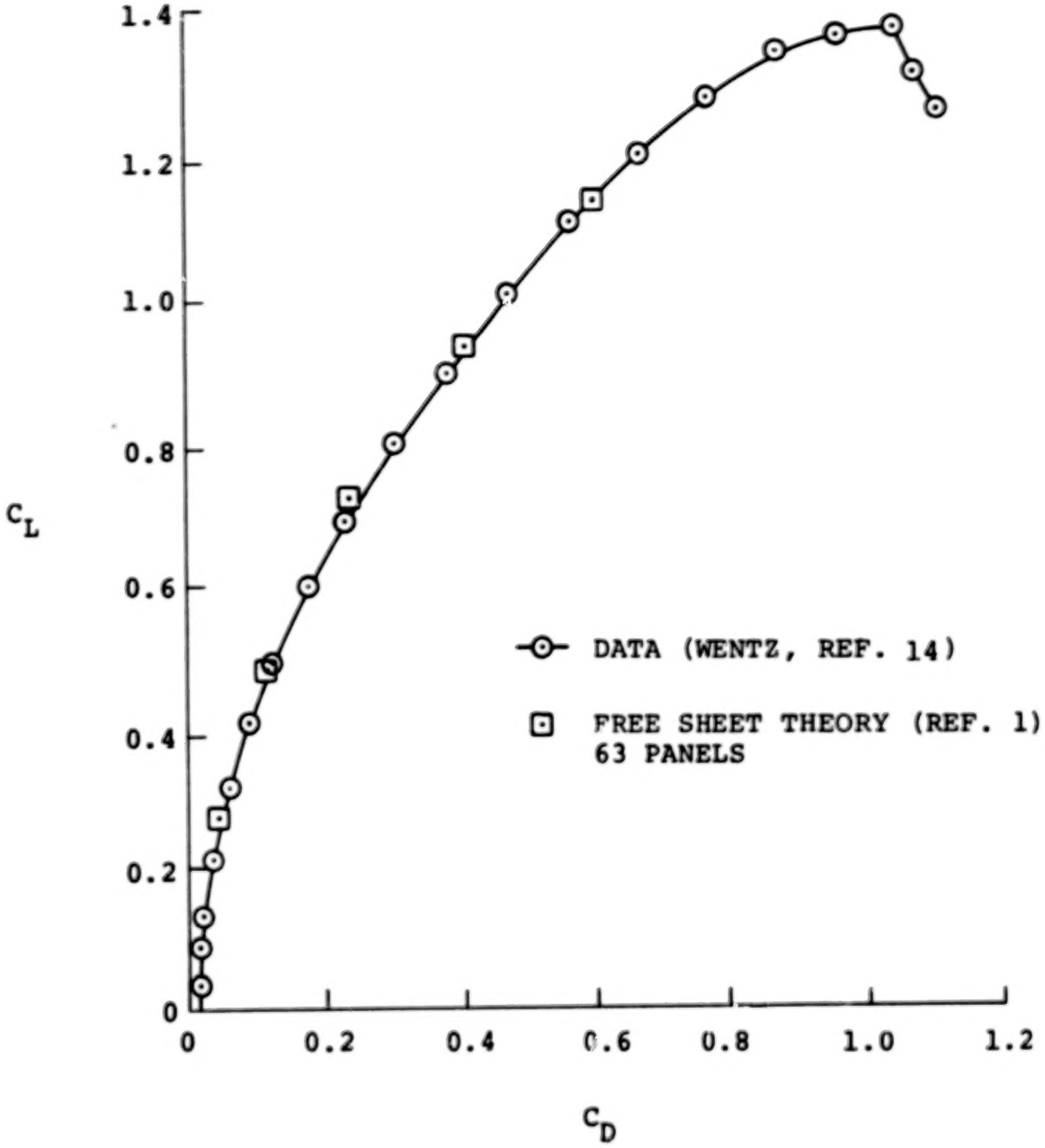

Figure 18. Drag polar comparison - conical camber delta, $M \cong 0$.

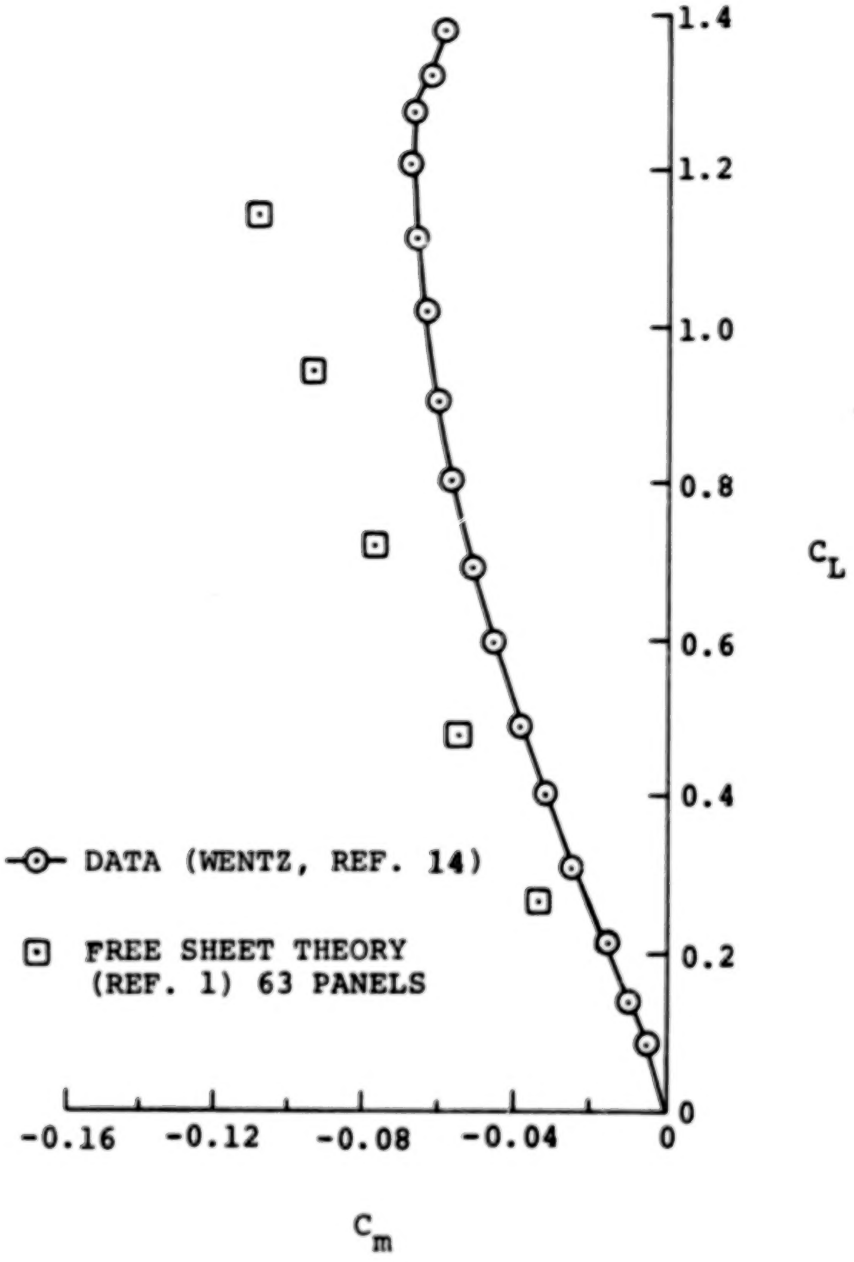

Figure 19. Pitch moment comparison - conical camber delta, $M \cong 0$.

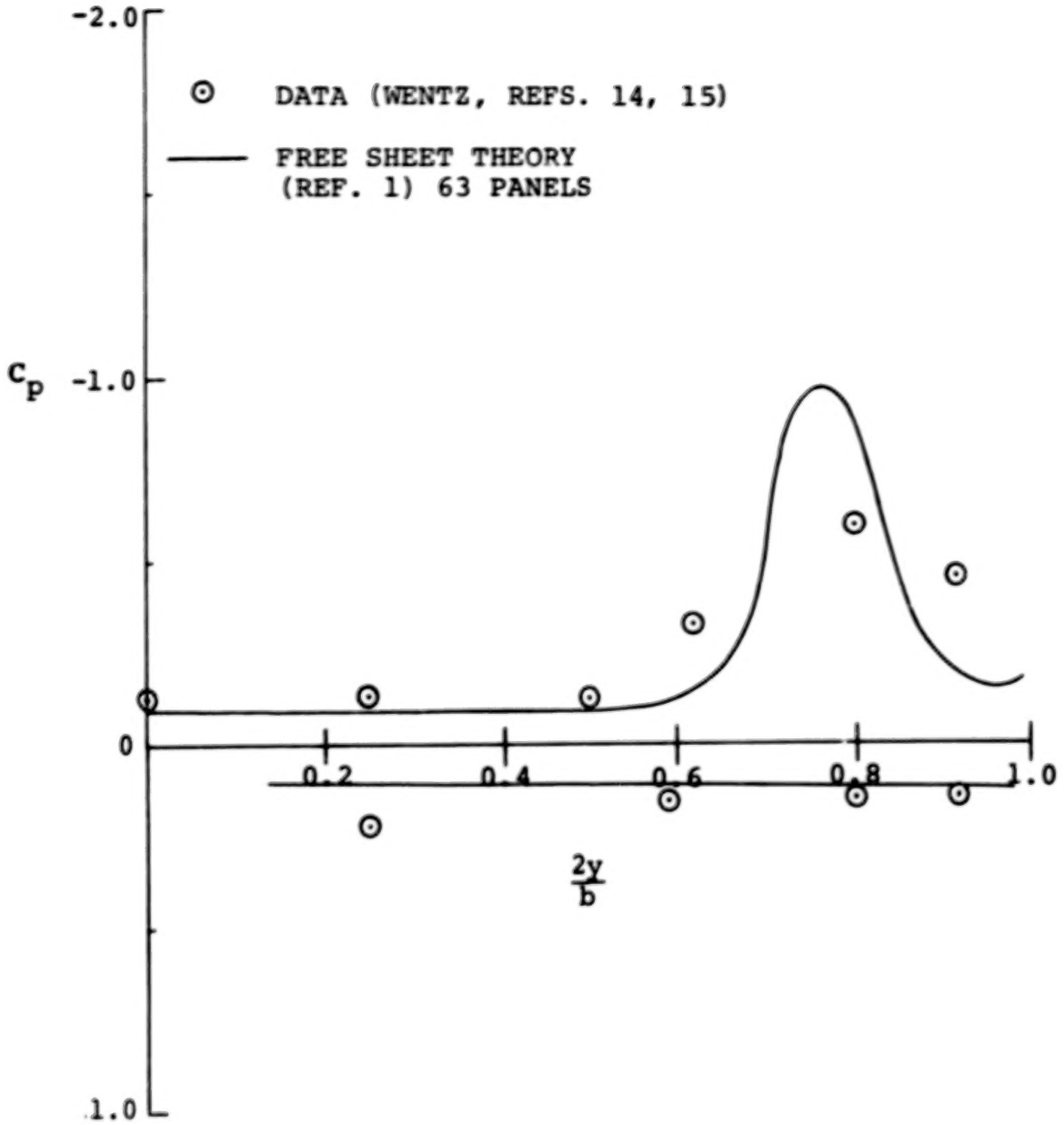

Figure 20. Pressure distribution, $\frac{x}{c_r} = 0.40$, $\alpha = 10.3°$, conical camber delta, $M \cong 0$.

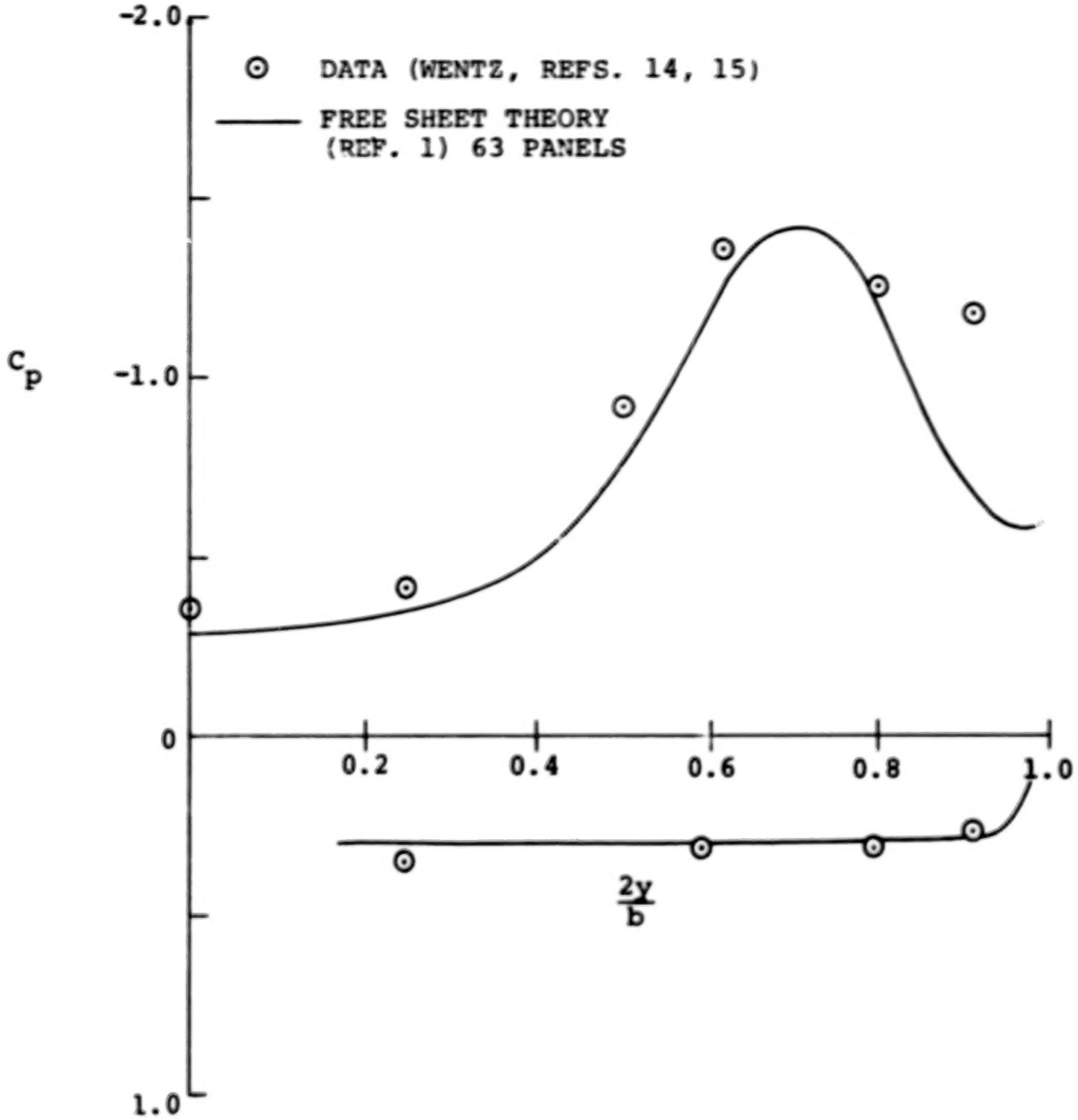

Figure 21. Pressure distribution, $\frac{x}{c_r} = 0.40$, $\alpha = 20.4°$, conical camber delta, $M \cong 0$.

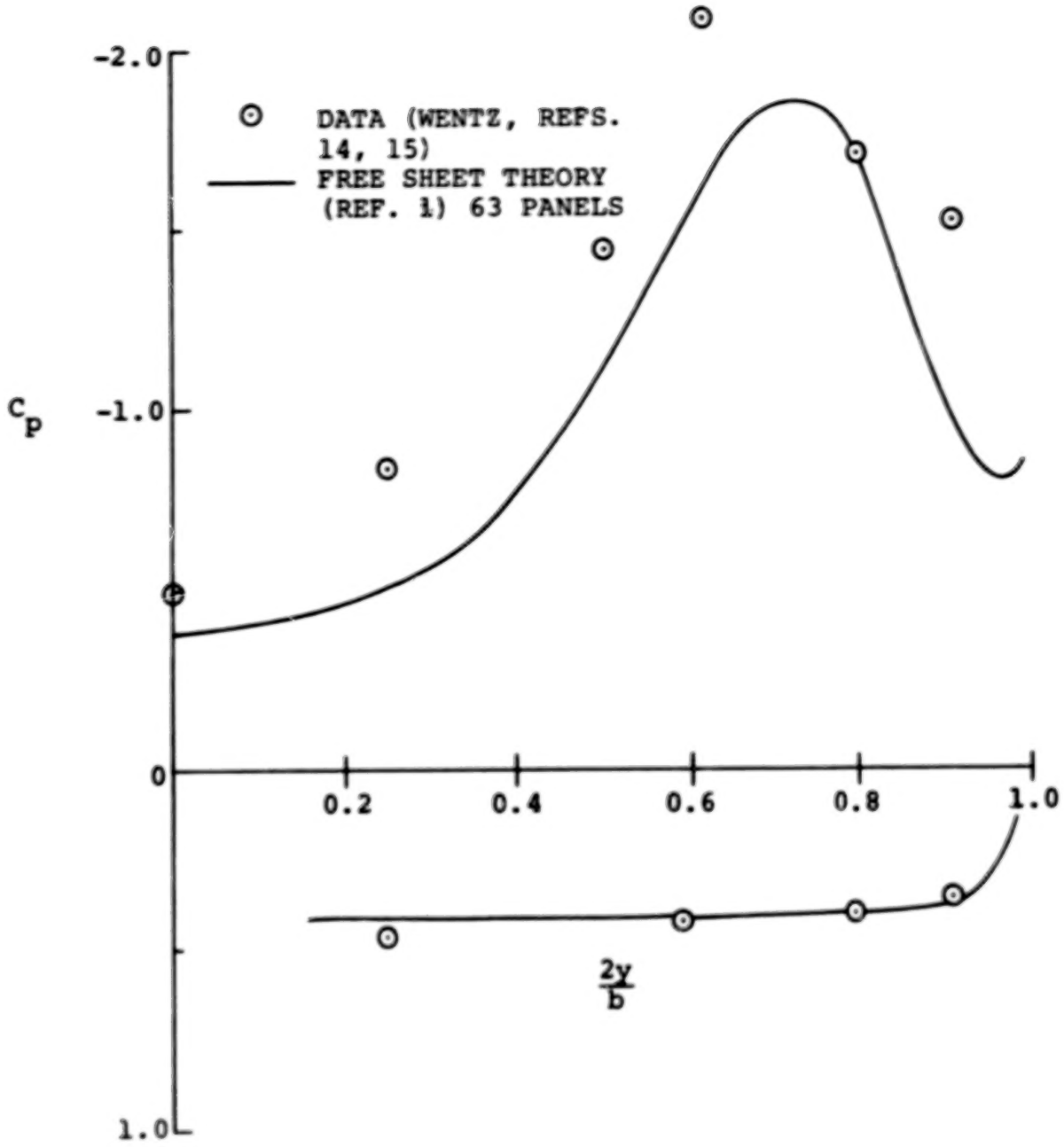

Figure 22. Pressure distribution, $\frac{x}{c_r} = 0.40$, $\alpha = 25.6°$, conical camber delta, $M \cong 0$.

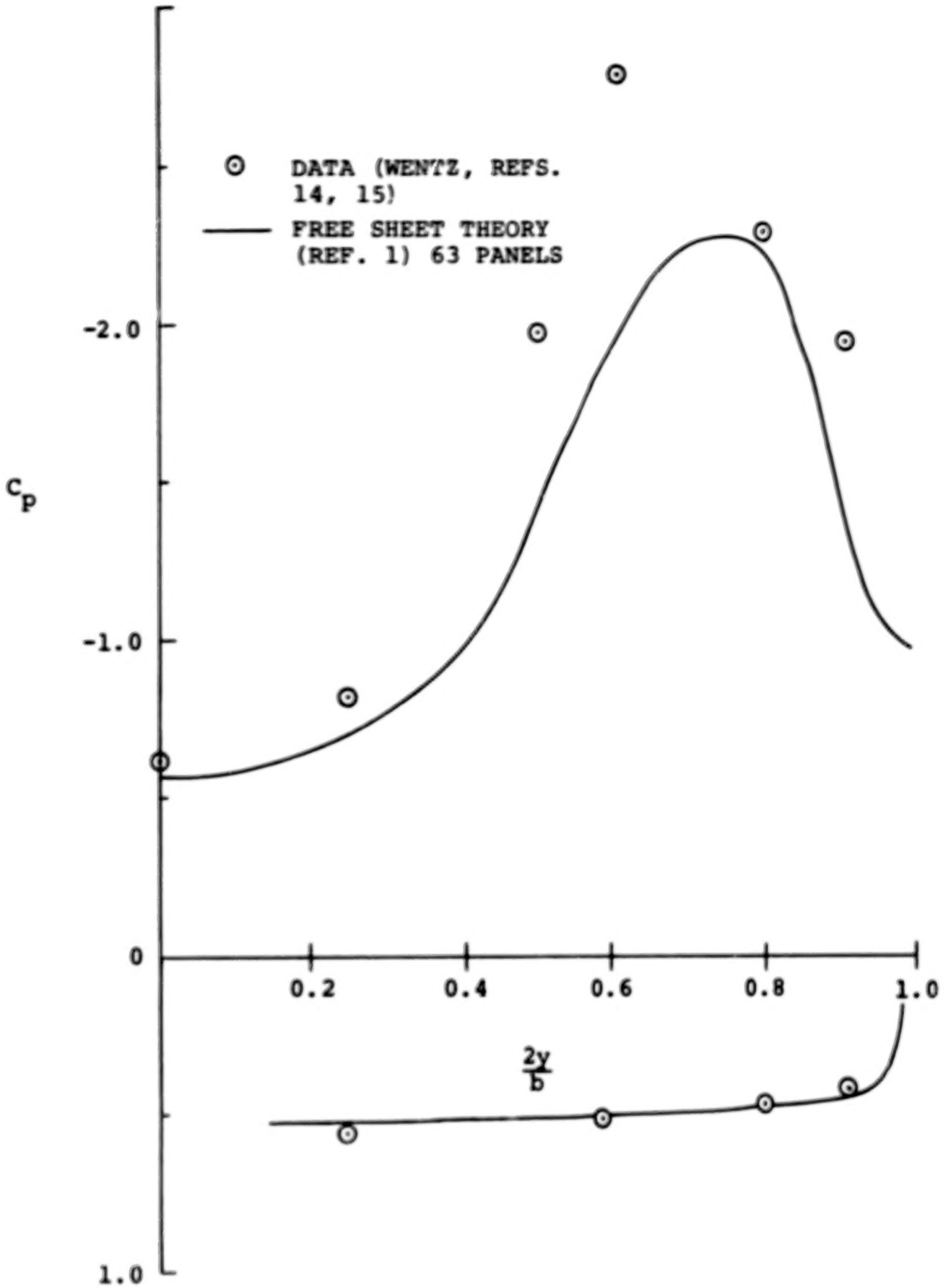

Figure 23. Pressure distribution, $\frac{x}{cr} = 0.40$, $\alpha = 30.7°$, conical camber delta, $M \cong 0$.

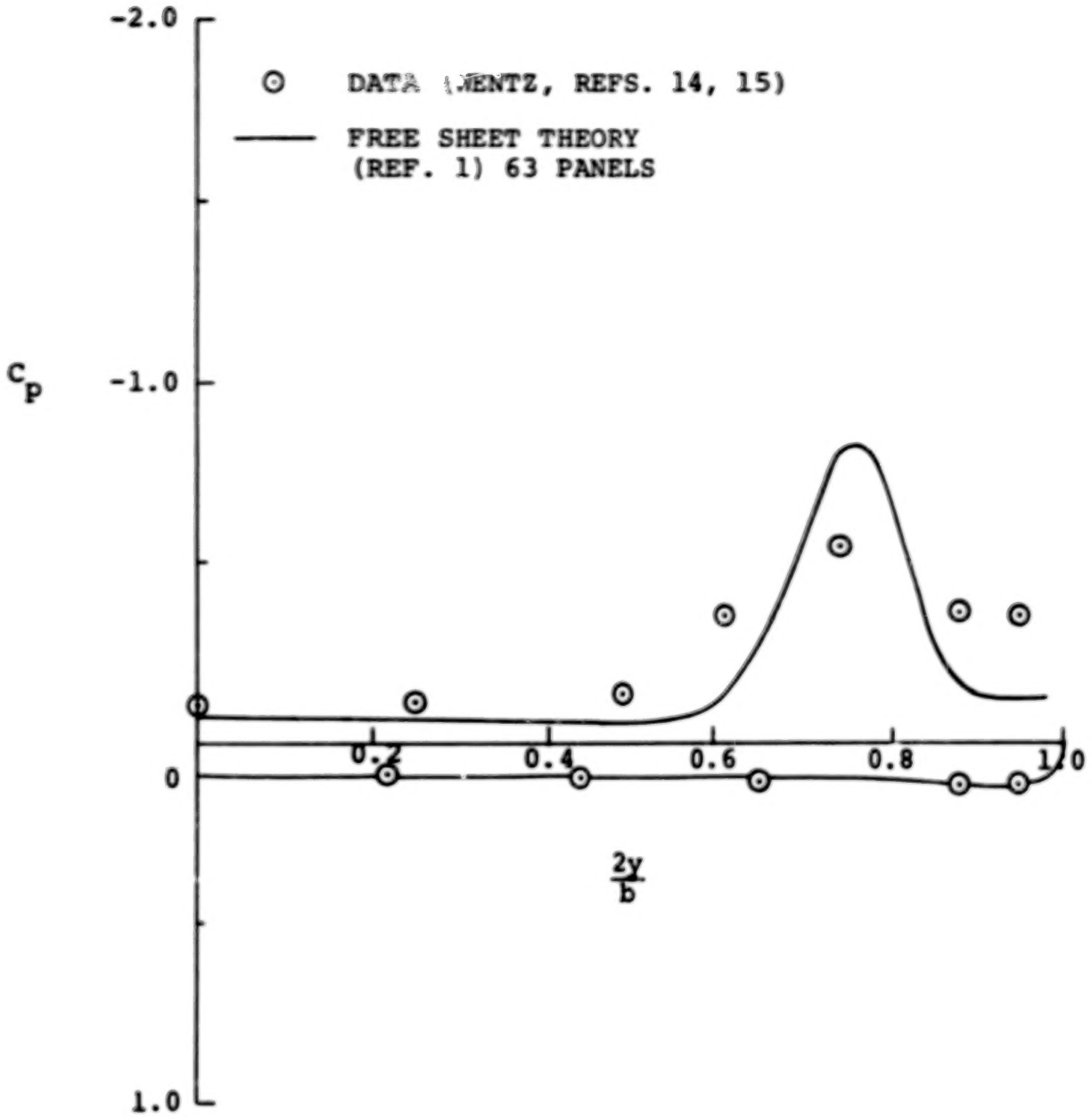

Figure 24. Pressure distribution, $\frac{x}{c_r} = 0.67$, $\alpha = 10.3°$, conical camber delta, $M \cong 0$.

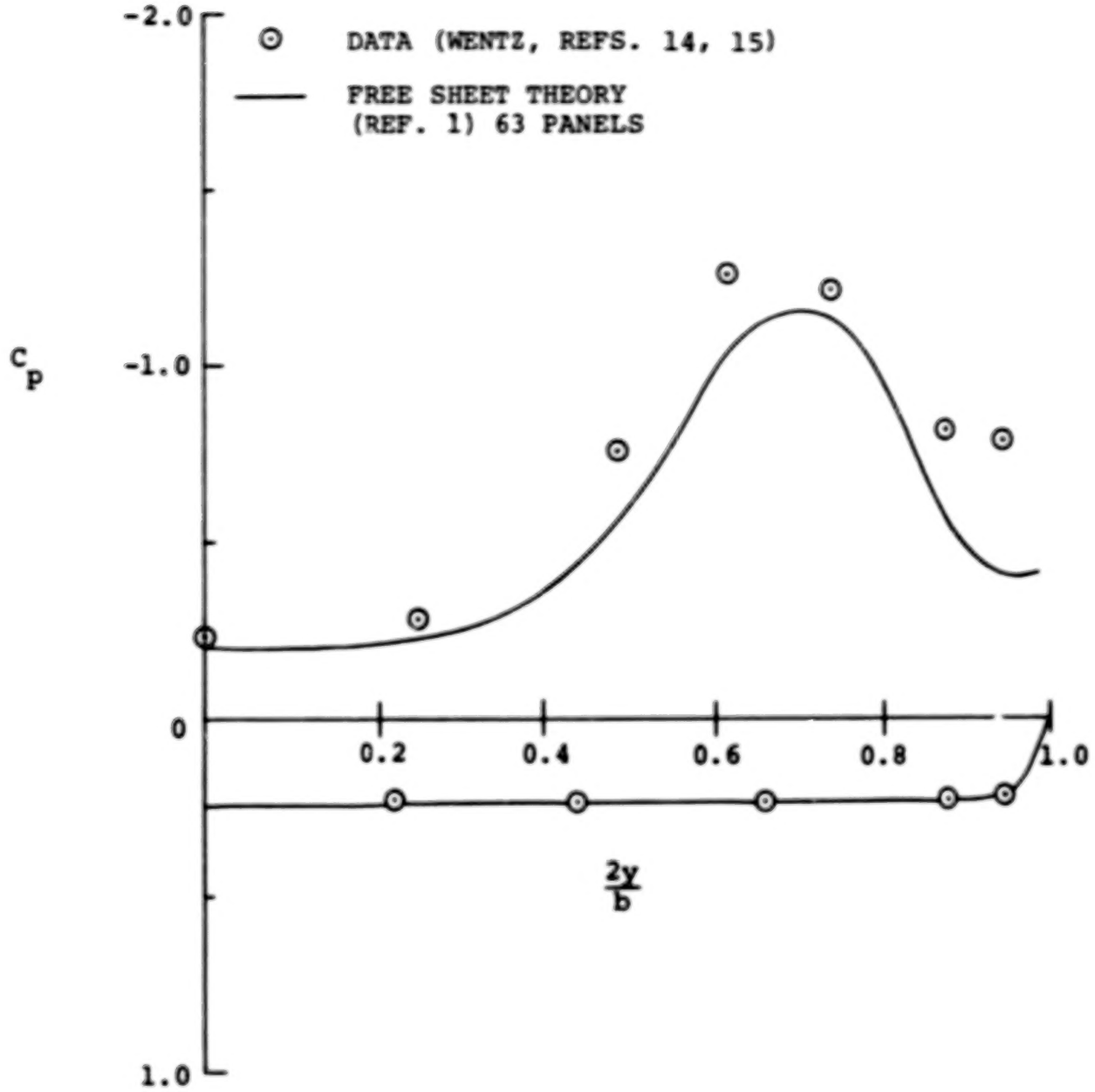

Figure 25. Pressure distribution, $\frac{x}{c_r} = 0.67$, $\alpha = 20.4°$, conical camber delta, $M \cong 0$.

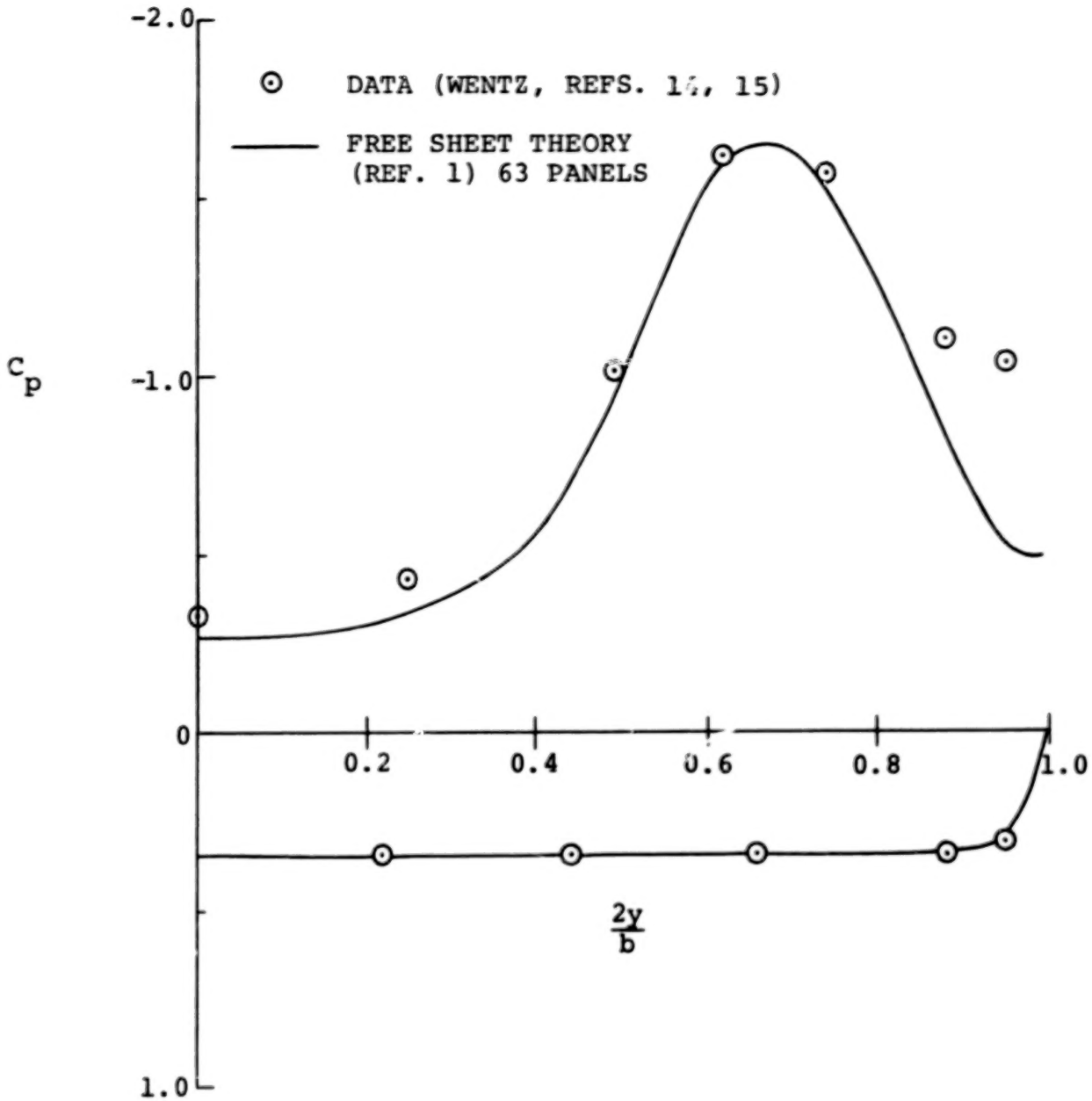

Figure 26. Pressure distribution, $\frac{x}{c_r} = 0.67$, $\alpha = 25.6°$, conical camber delta, $M \cong 0$.

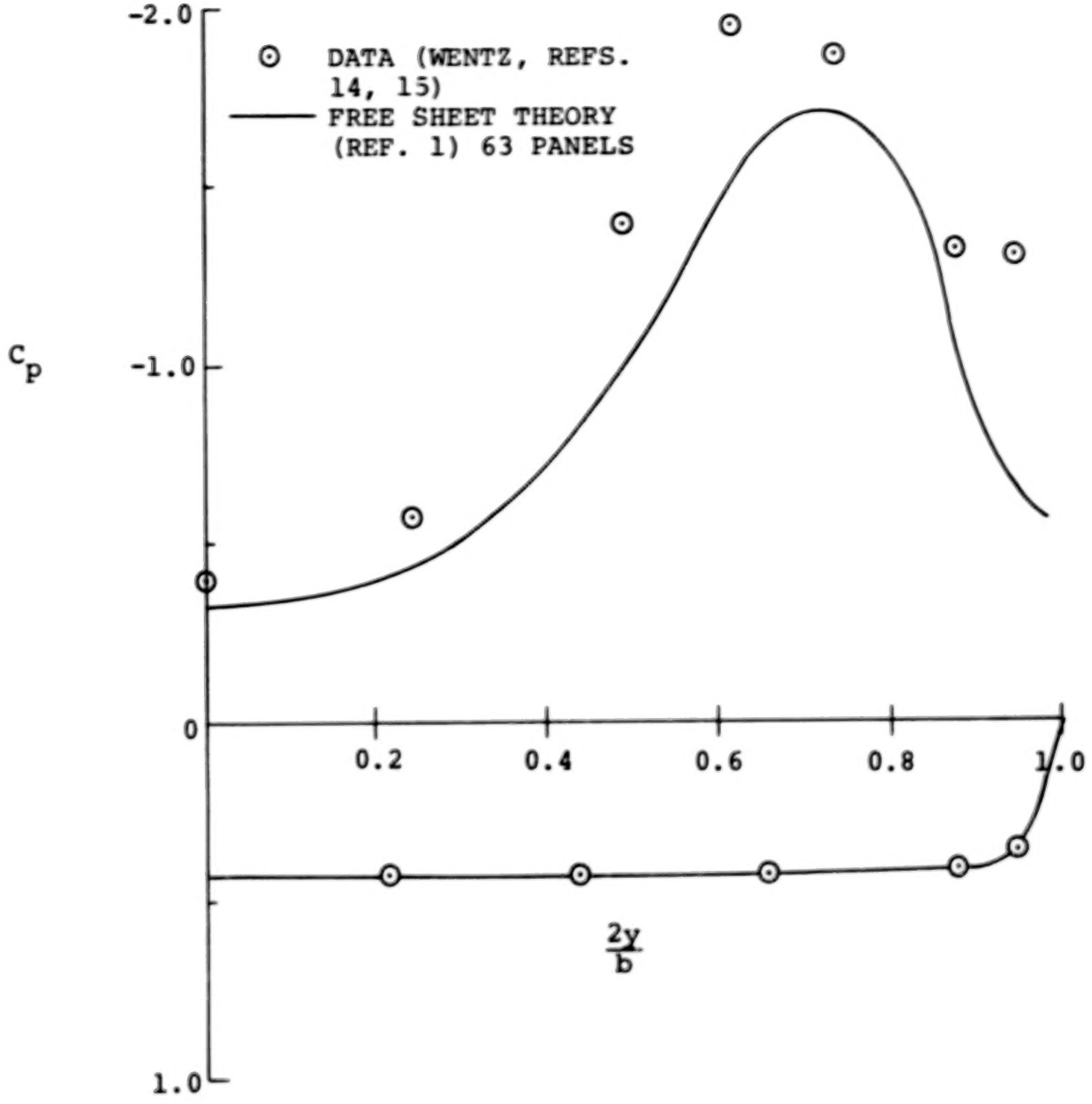

Figure 27. Pressure distribution, $\frac{x}{c_r} = 0.67$, $\alpha = 30.7°$, conical camber delta, $M \cong 0$.

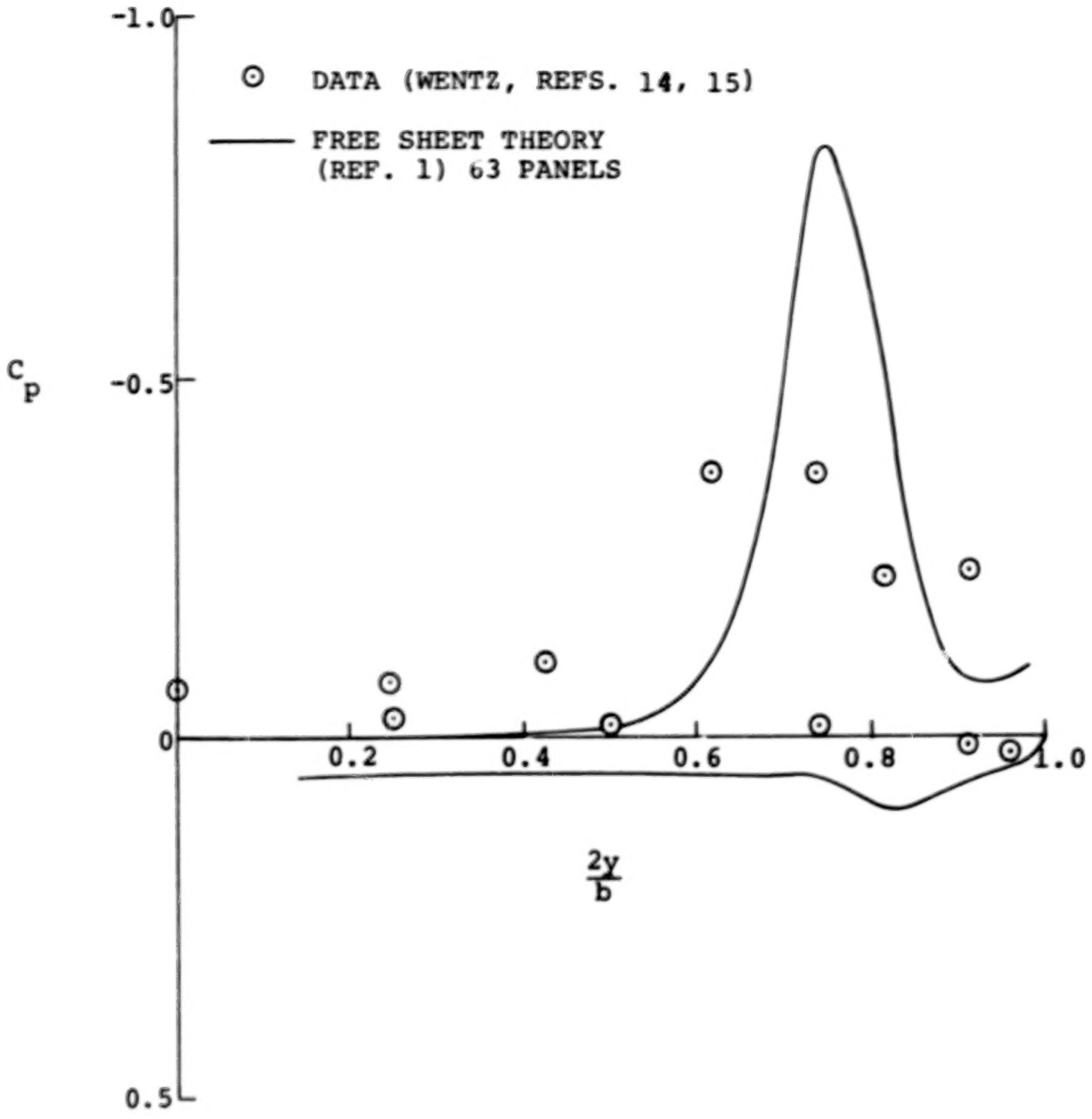

Figure 28. Pressure distribution, $\frac{x}{c_r} = 0.935$, $\alpha = 10.3°$, conical camber delta, $M \cong 0$.

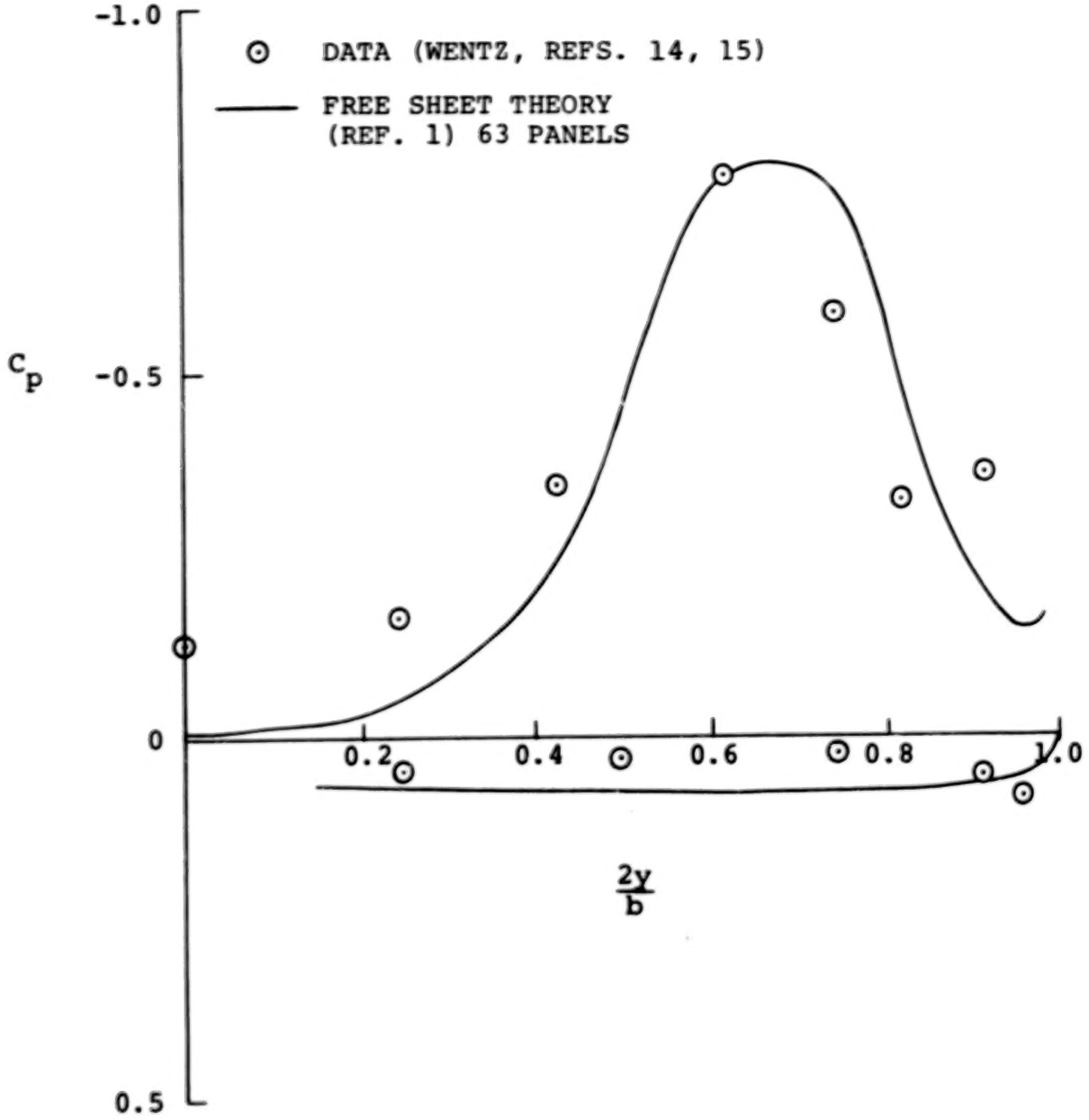

Figure 29. Pressure Distribution, $\frac{x}{c_r} = 0.935$, $\alpha = 20.4°$, conical camber delta, $M \cong 0$.

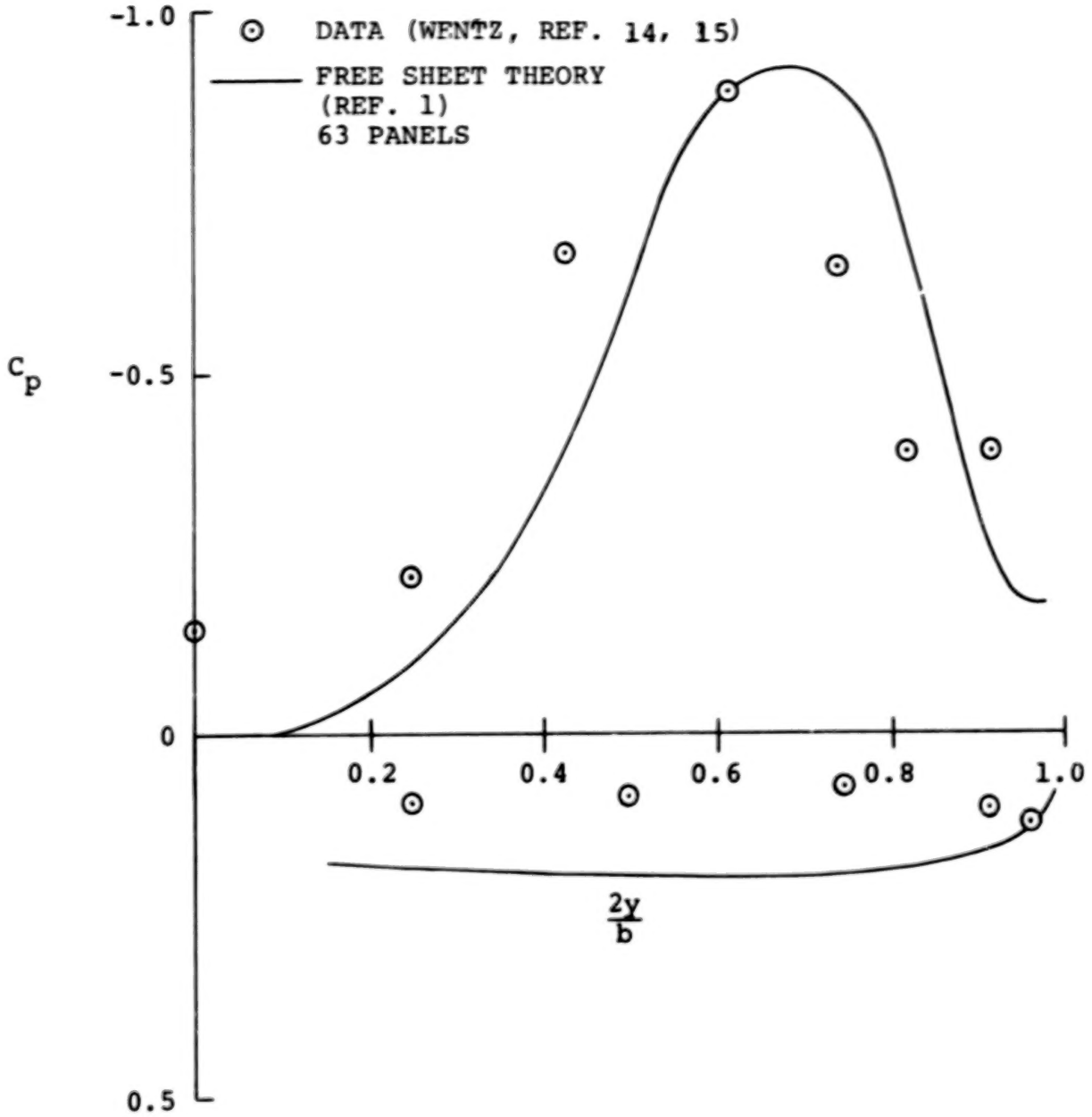

Figure 30. Pressure distribution, $\frac{x}{c_r} = 0.935$, $\alpha = 25.6°$, conical camber delta, $M \cong 0$.

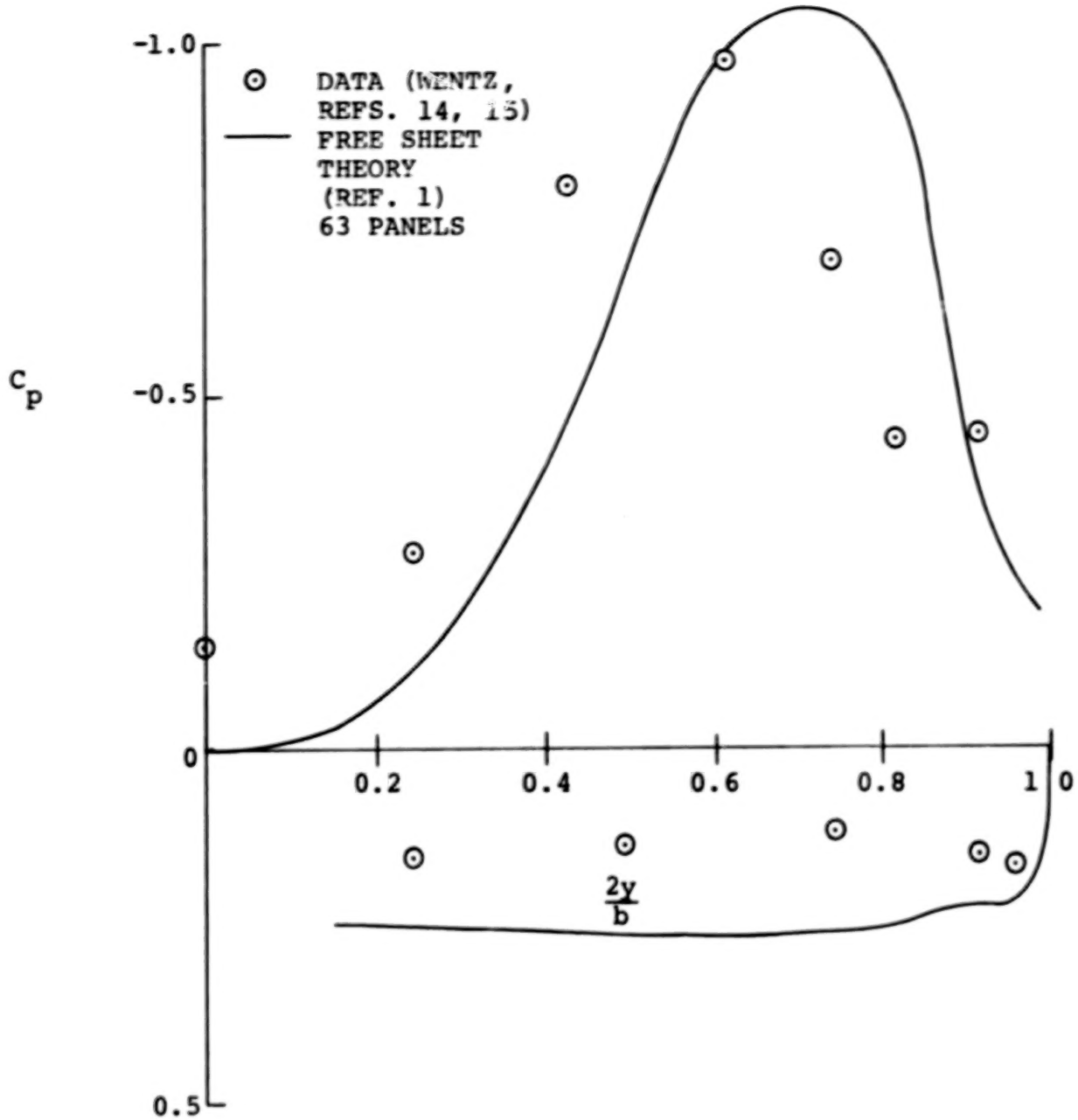

Figure 31. Pressure distribution, $\frac{x}{c_r} = 0.935$, $\alpha = 30.7°$, conical camber delta, $M \cong 0$.

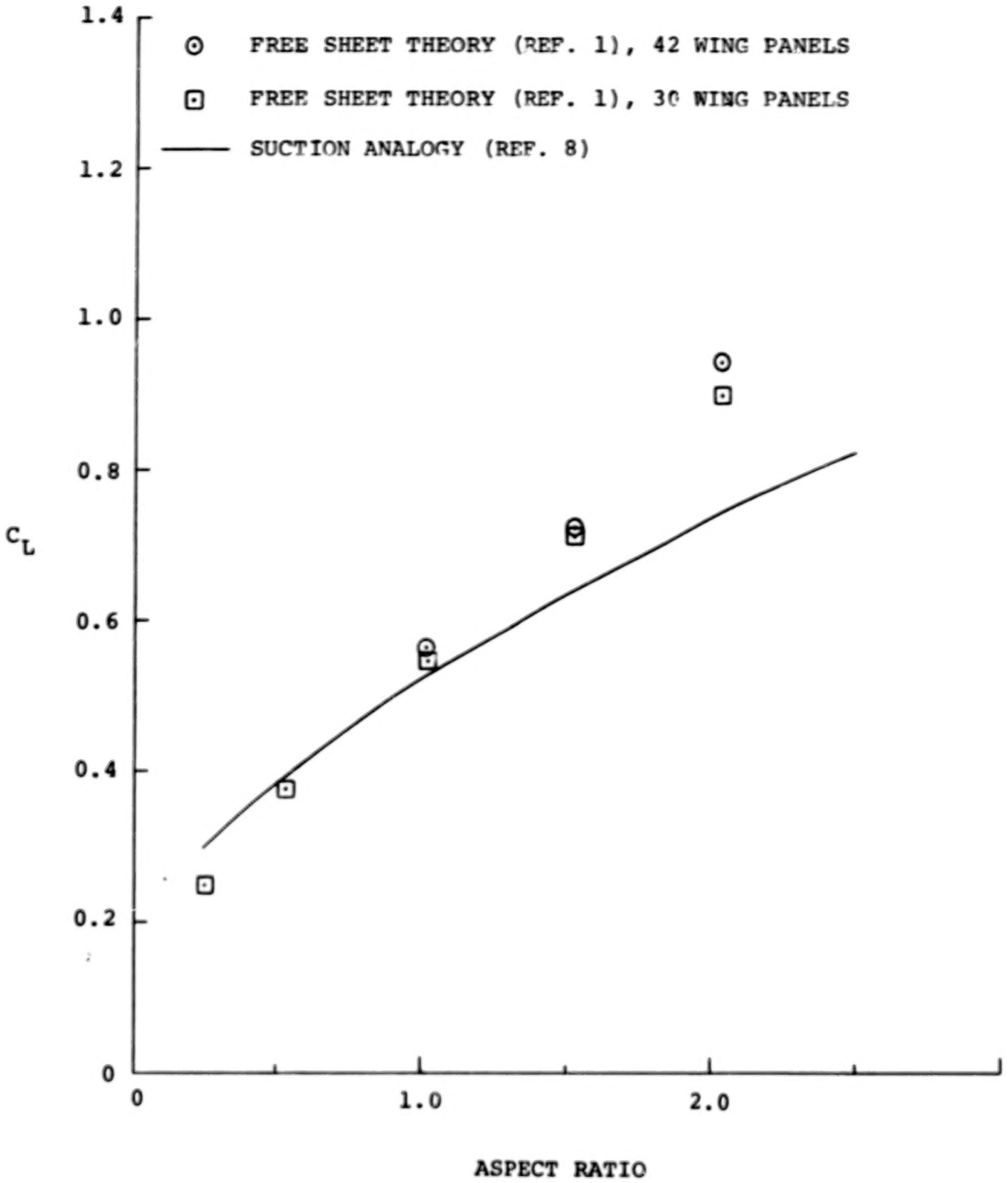

Figure 32. Lift coefficient variation with aspect ratio for flat delta wings at M = 0, α = 15°.

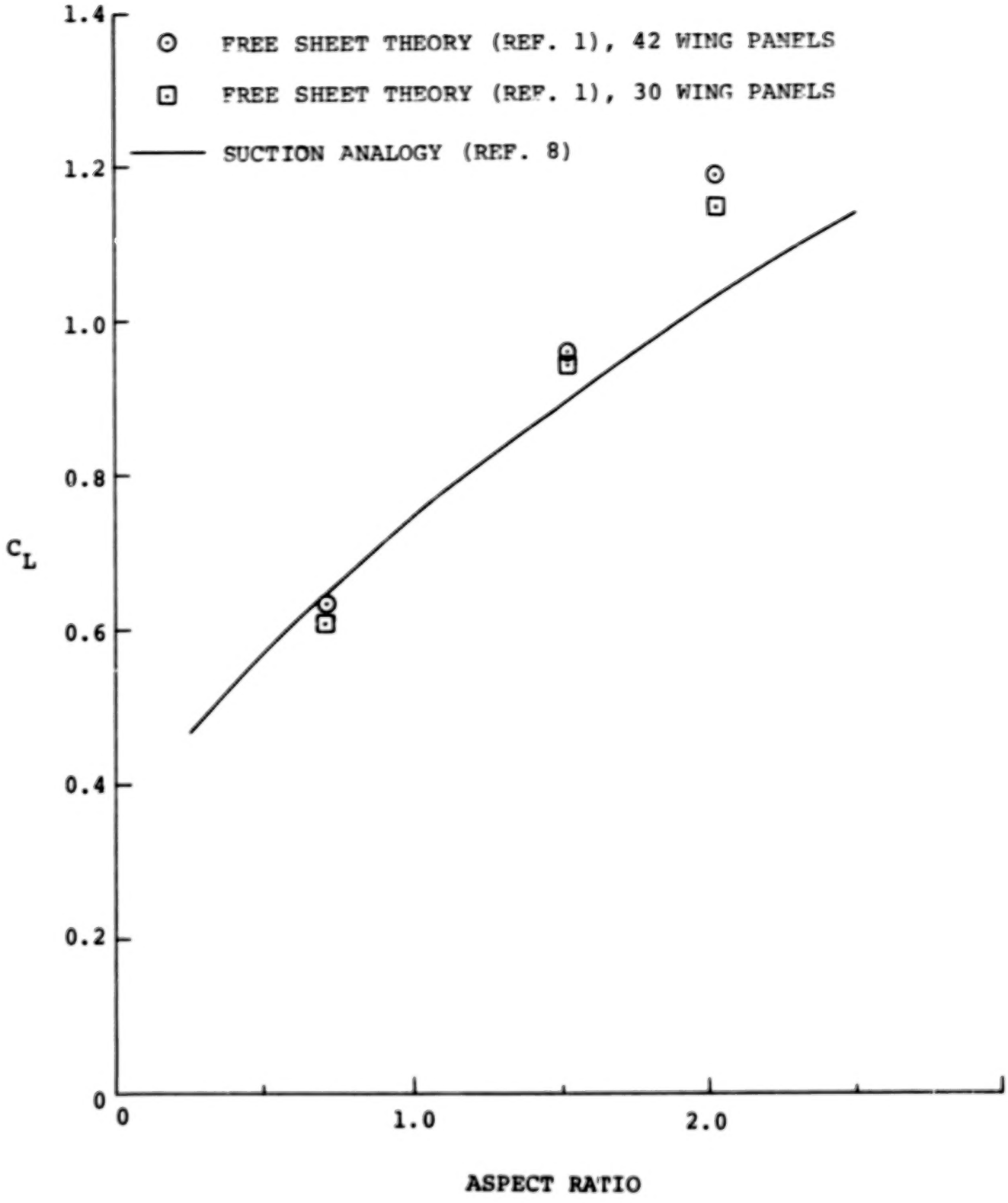

Figure 33. Lift coefficient variation with aspect ratio for flat delta wings at M = 0, α = 20°.

1. Report No.	2. Government Accession No.	3. Recipient's Catalog No.
NASA CR-3022		

4. Title and Subtitle	5. Report Date
Analytical Studies of Separated Vortex Flow on Highly Swept Wings	November 1978
	6. Performing Organization Code

7. Author(s)	8. Performing Organization Report No.
John M. Kuhlman	
	10. Work Unit No.
9. Performing Organization Name and Address	
Old Dominion University Research Foundation Norfolk, Virginia 23508	11. Contract or Grant No. NSG 1357
	13. Type of Report and Period Covered Contractor Report
12. Sponsoring Agency Name and Address	
National Aeronautics and Space Administration Langley Research Center Hampton, Virginia 23665	14. Sponsoring Agency Code

15. Supplementary Notes

Langley Technical Monitor: John E. Lamar

Topical Report

16. Abstract

An investigation has been conducted into the capabilities of a subsonic potential flow mathematical model of the flow past slender aerodynamic surfaces with sharp edges and separated vortex flow. Comparisons with experimental data are presented for overall forces and pressure distributions for a series of thin, low aspect ratio wings, including both flat and conically cambered ones. A discussion is presented of the limitations of the current theory, and some suggestions are made as to how the theory might be improved. Details of program data input modifications for three-dimensional geometry are described in an appendix.

17. Key Words (Suggested by Author(s))	18. Distribution Statement
Aerodynamics Delta wings Vortex flow High angle of attack	Unclassified - Unlimited Subject Category: 02

19. Security Classif. (of this report)	20. Security Classif. (of this page)	21. No. of Pages	22. Price*
Unclassified	Unclassified	62	$5.25

* For sale by the National Technical Information Service, Springfield, Virginia 22151

NASA-Langley, 1978

END

FEB 28, 1979